Inorganica Chimica Acta 574 (2025) 122394

Contents lists available at ScienceDirect

Inorganica Chimica Acta

journal homepage: www.elsevier.com/locate/ica

Molecular hydride carbonyl clusters and nanoclusters

Cristiana Cesari, Cristina Femoni, Francesca Forti, Maria Carmela Iapalucci, Giorgia Scorzoni, Stefano Zacchini *

Dipartimento di Chimica Industriale "Toso Montanari", Università di Bologna, Via P. Gobetti 85, 40129 Bologna, Italy

ARTICLE INFO

Dedicated to Professor Alberto Albinati in recognition of his contribution to the chemistry of metal hydrides and molecular metal clusters.

Keywords:
Cluster compounds
Carbonyl ligands
Hydride ligand
Molecular nanoclusters
Metal hydrides

ABSTRACT

This minireview outlines the actual status of the chemistry of hydride metal carbonyl clusters (MCCs) by means of pertinent examples, without being comprehensive. After a brief introduction to the topic, the major synthetic routes for the introduction of hydride ligands in MCCs are described, with particular focus on the different typologies of reagents that can be employed. The structures of hydride MCCs and the different coordination modes of hydride ligands are, then presented, based on single-crystal X-ray and neutron diffraction data available. Some general considerations on ^{1}H NMR studies of hydride MCCs are described, including fluxionality and the problems of detecting hydrides in larger MCCs. Moreover, electrochemical studies of hydride MCCs are summarized, focusing on electrochemistry as an indirect tool for determining the hydride nature of large MCCs, and tuning the redox potentials of MCCs by protonation/deprotonation reactions. Applications of hydride MCCs in catalysis and electrocatalysis are only briefly described at the end of this minireview, since this topic has been recently reviewed.

1. Introduction

Metal hydrides are ubiquitous in chemistry, and find several applications in material sciences, nanochemistry and nanosciences, homogeneous and heterogeneous catalysis, organic synthesis, and hydrogen storage [1–3]. From a fundamental point of view, hydrogen has a unique chemistry, in view of its small mass, the presence of a single 1 s valence orbital, the absence of core and non-bonding electrons, and an anomalously high electronegativity [4]. These factors contribute to the versatility of the M−H interaction, depending on the nature of the metal, the size of the aggregate, the presence of ancillary ligands and heteroatoms. Several mononuclear and polynuclear hydride metal complexes are known, involving transition metals, f-block metals, and main group elements [5–8]. This is paralleled by the very extended chemistry of bulk metal hydrides. Several studies have been also dedicated to the interactions of hydrogen with metal surfaces and metal nanoparticles [9,10].

The chemistry of molecular hydride nanoclusters of coinage metals has been developed only very recently, boosting a renewed interest for atomically precise hydride metal nanoclusters [11–13]. It must be remarked that the first hydride carbonyl metal complexes, that is, $[HCo(CO)_4]$ and $[H_2Fe(CO)_4]$, have been discovered by Hieber in the 1930s [14]. In the following five decades, the chemistry of molecular hydride metal carbonyl clusters (MCCs) has considerably grown [15–21]. This helped understanding the fundamental binding modes of H-atoms to metal clusters, and prompted the development of the cluster surface analogy [22]. Neutron diffraction studies [23] showed that $[H_4Os_{10}(CO)_{24}]^{2-}$ contains two edge-bridging (μ-H) and two face-capping (μ_3-H) hydride ligands [24], whereas fully interstitial hydrides are present in $[HCo_6(CO)_{15}]^{-}$ [25], $[HNi_{12}(CO)_{21}]^{3-}$, $[H_2Ni_{12}(CO)_{21}]^{2-}$ [26], and $[HRu_6(CO)_{18}]^{-}$ [27]. The species $[H_2Rh_{13}(CO)_{24}]^{3-}$ displays, instead, semi-interstitial hydride ligands [28]. Variable temperature (VT) ^{1}H NMR studies have clearly demonstrated that often hydride MCCs are fluxional, and the H-atoms may migrate on the surface of the cluster or diffuse within its metal cage, depending on the nature and size of the cluster. Even though most of the clusters reported so far contain 3–13 metal atoms, also nanometric hydride MCCs have been characterized. For instance, Dahl *et al.* reported the very large $[H_{12}Pd_{28}(PtPMe_3)(PtPPh_3)_{12}(CO)_{27}]$, which has been described as a hydrogen storage model for Pd metal [29]. Further examples will be reported in the following Sections.

This minireview is not intended to be comprehensive, but attempts to give some general outlines on the state of the art of the chemistry of hydride MCCs. Particular focus will be given to clusters of increasing sizes. After this brief introduction, Section 2 will be dedicated to the synthesis of hydride MCCs, particularly regarding the different

* Corresponding author.
E-mail address: stefano.zacchini@unibo.it (S. Zacchini).

https://doi.org/10.1016/j.ica.2024.122394
Received 23 July 2024; Received in revised form 16 September 2024; Accepted 25 September 2024
Available online 26 September 2024

strategies employed in order to introduce hydride ligands in MCCs. Section 3 will deal with the structures of hydride MCCs and the different coordination modes of hydride ligands to MCCs, mainly obtained from single-crystal X-ray diffraction data (SC-XRD), but also neutron diffraction experiments. Section 4 will present NMR studies of hydride MCCs, including fluxionality and the problems of detecting hydrides in larger MCCs. Section 5 will deal with electrochemical studies, focusing on electrochemistry as an indirect tool for determining the hydride nature of large MCCs, and tuning the redox potentials of MCCs by protonation/deprotonation reactions. Section 6 will briefly outline applications of hydride MCCs in catalysis and electrocatalysis, since this topic has been recently reviewed [30]. Some general conclusions will be outlined in Section 7.

2. Synthesis

Hydride ligands can be introduced into MCCs using different reagents [31]:

(a) Metal and boron hydrides, *e.g.*, $NaBH_4$;
(b) Molecular hydrogen, H_2;
(c) Protic acids, *e.g.*, H_2SO_4, HBF_4, CF_3SO_3H, H_3PO_4;
(d) Water and traces of moisture;
(e) Organic solvents and organic molecules;
(f) Nucleophilic attack of OH^- ions at M−bonded CO followed by CO_2 elimination and migration of a hydrogen atom on the metal cage;
(g) Metal hydride carbonyl complexes or modification of preformed hydride MCCs.

From a mechanistic point of view, hydride ligands may enter into a MCC as H^- or H^+ ions, or H-radicals. Nonetheless, since the mechanism is rarely known, the following discussion will be mainly based on the nature of the reagent employed. It must be remarked that entries (c), (d) and (e) in the list consist mainly of molecules that can be viewed as proton donors and, therefore, they will be treated together in the following discussion (Section 2.2). In the case (e), sometimes H-atoms may be abstracted from organic molecules as H-radicals or even as hydrides.

Because of the π-acidic nature of CO, hydride ligands in metal carbonyls and MCCs often behave as protons more than hydrides. Indeed, it is well known that $[HCo(CO)_4]$ behaves as a strong acid and easily dissociates into H^+ and $[Co(CO)_4]^-$. This behavior is rather common, and protonation/deprotonation reactions by means of acids/bases are ubiquitous in MCC chemistry. Several examples will be reported in the following discussion. Because of this, hydride ligands in MCCs often originate from protic compounds, such as acids, water and alcohols.

From a practical point of view, it must be remarked that the synthetic pathways (c) and (d) are probably the most viable starting from anionic MCCs. These procedures can be used in order to introduce hydride ligands in non-hydride MCCs, or to increase the number of hydride ligands in preformed hydride MCCs. Synthetic pathway (b) is more often used starting from neutral MCC, even though some applications to anionic MCCs are known. Synthetic routes (b), (c) and (d) can be used, also, in order to obtain larger hydride MCCs, starting from lower nuclearity carbonyl species. Route (a) is very limited, and only a few examples are known, involving neutral MCCs as starting materials. Also procedure (e) is usually adopted starting from neutral MCCs. Synthetic route (f) may be applied to both neutral and anionic MCCs, even if the final products may be or may be not hydride MCCs. Synthetic route (g) is rather general, and usually adopted in order to introduce organic ligands or metal–ligand fragments in preformed hydride MCCs, or to obtain larger hydride MCCs starting from smaller ones.

As noticed above, syntheses of hydride MCCs employing conventional hydride species (entry (a) of the list) are rather rare. The most significant examples are the reactions of $[Ru_3(CO)_{12}]$ and $[Os_6(CO)_{18}]$ with $NaBH_4$ yielding $[HRu_3(CO)_{11}]^-$ [32,33] and $[HOs_6(CO)_{18}]^-$ [34], respectively (Fig. 1). It must be remarked that in both cases the syntheses start from neutral MCCs and generate anionic species formally arising from the addition of a H^- ion with or without CO elimination.

2.1. Syntheses of hydride MCCs using molecular hydrogen

The reaction of a MCC with H_2 (entry (b) of the list) may proceed *via* substitution of one or more CO ligands with hydrides, with or without structural rearrangement of the metal cage, including also variations of its nuclearity. It must be remarked that, from the point of view of the electron count, one CO ligand donates two electrons, as two hydrides.

For instance, one CO ligand of $[HRu_3(\mu\text{-}COMe)(CO)_{10}]$ is replaced by two hydrides upon exposure to H_2 (reaction (1) [35]. The process may be reversed by adding CO, and the kinetic of the reaction has been spectroscopically investigated.

$$[HRu_3(\mu - COMe)(CO)_{10}] + H_2 \leftrightarrow [H_3Ru_3(\mu - COMe)(CO)_9] + CO \qquad (1)$$

As a further example, four CO ligands of $[Ir_4(CO)_8(PPh_3)_4]$ are replaced by eight hydrides upon reaction with H_2 resulting in $[H_8Ir_4(CO)_4(PPh_3)_4]$ [36]. The same species may be obtained from the direct reaction of $[Ir_4(CO)_{12}]$ with H_2 and PPh_3 in toluene at 90 °C (Fig. 2).

The reaction of the electron precise $[Os_3(CO)_{12}]$ (48 CVE) with H_2 (1 atm) in octane results in the unsaturated species $[H_2Os_3(CO)_{10}]$ (46 CVE) upon replacement of two carbonyls with two hydride ligands (Scheme 1) [37]. It must be remarked that, employing H_2 at higher pressure (60 atm) in refluxing heptane, $[Os_3(CO)_{12}]$ is transformed into the higher nuclearity poly-hydride $[H_4Os_4(CO)_{12}]$. Interestingly, $[Ru_3(CO)_{12}]$ is transformed into $[H_4Ru_4(CO)_{12}]$ under milder conditions (H_2 1 atm, octane, reflux), without the formation of any unsaturated species.

In some cases, structural rearrangements may occur after reaction with H_2. This may lead to complex mixtures of products as in the case of the reaction of $[Pt_2Os_4(CO)_{18}]$ with H_2 (100 atm, 25 °C) that results in $[H_6PtOs_5(CO)_{16}]$, $[H_6Pt_2Os_5(CO)_{17}]$, $[H_8PtOs_6(CO)_{18}]$, and $[H_8Pt_2Os_7(CO)_{23}]$, that may be separated by TLC (Fig. 3) [38].

As suggested by Paolo Chini [19], selectivity of thermal reactions of MCCs, including those with H_2, may be increased using anionic rather than neutral clusters. MCC anions may be also generated *in situ* by using bases or reducing agents. For instance, reaction of $[Rh_4(CO)_{12}]$ in refluxing ^{i}PrOH under H_2 atmosphere in the presence of NaOH affords

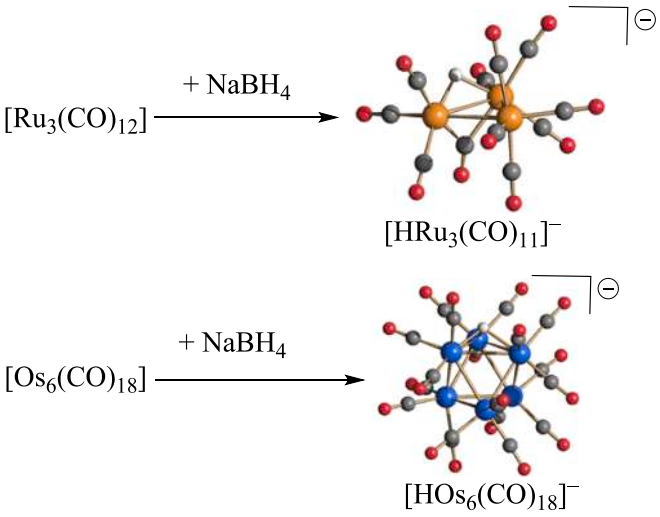

Fig. 1. Synthesis of $[HRu_3(CO)_{11}]^-$ and $[HOs_6(CO)_{18}]^-$ employing $NaBH_4$ as hydride source (orange, Ru; blue, Os; red, O; grey, C; white, H). $[HRu_3(CO)_{11}]^-$ contains one μ-H ligand, $[HOs_6(CO)_{18}]^-$ a μ_3-H.

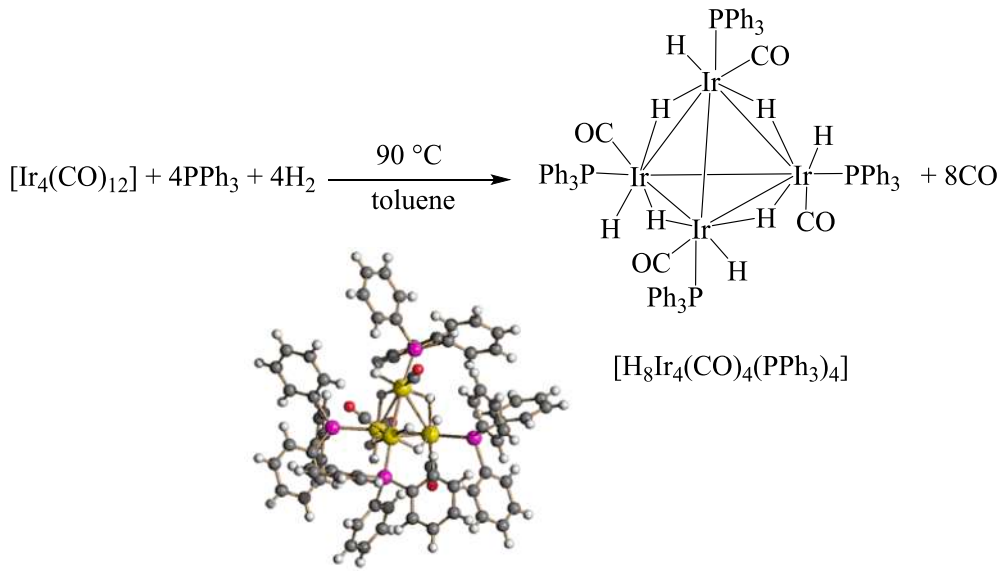

Fig. 2. Synthesis of $[H_8Ir_4(CO)_4(PPh_3)_4]$ by replacement of eight CO ligands of $[Ir_4(CO)_{12}]$ with four PPh_3 and eight hydrides, the latter originated from four H_2 molecules (yellow, Ir; purple, P; red, O; grey, C; white, H). The cluster contains four terminal and four edge bridging hydrides.

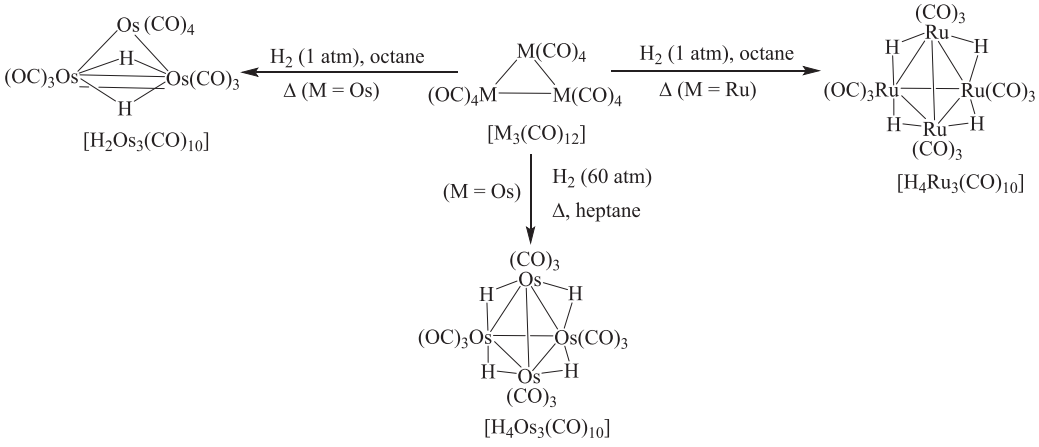

Scheme 1. The reactions of $[M_3(CO)_{12}]$ (M = Ru, Os) with H_2 afford different products depending on the experimental conditions.

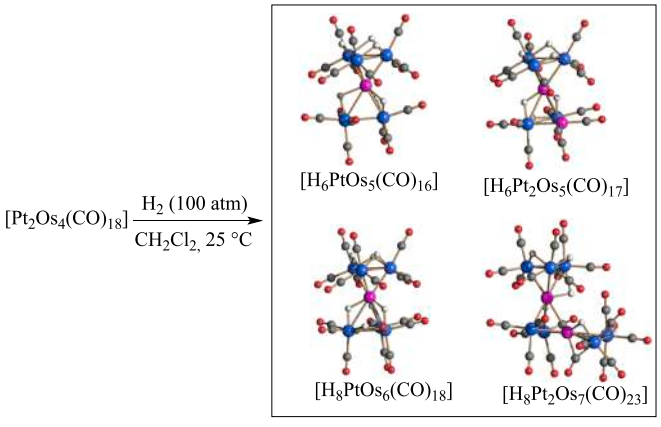

Fig. 3. The reaction of $[Pt_2Os_4(CO)_{18}]$ with H_2 (100 atm) affords a mixture of $[H_6PtOs_5(CO)_{16}]$, $[H_6Pt_2Os_5(CO)_{17}]$, $[H_8PtOs_6(CO)_{18}]$, and $[H_8Pt_2Os_7(CO)_{23}]$ (purple, Pt; blue, Os; red, O; grey, C; white, H). All hydrides are in edge bridging positions. The products can be separated by TLC.

$[H_2Rh_{13}(CO)_{24}]^{3-}$ (Fig. 4) [39]. The higher nuclearity MCC $[H_3Rh_{22}(CO)_{35}]^{5-}$ has been obtained as side product during the synthesis of $[H_2Rh_{13}(CO)_{24}]^{3-}$, and the two species separated owing their different solubilities in organic solvents [40].

Hydride MCCs may be also synthesized by reductive carbonylation under a combined CO/H_2 pressure. For instance, $[H_2Rh_{13}(CO)_{24}]^{3-}$ has been obtained from $[Rh(CO)_2(acac)]$ and PhCOOCs in diglyme at 140 °C under pressure of CO/H_2 (12 atm). This product is obtained using a very short reaction time (*ca.* 5 min), since longer reaction times lead to $[Rh_{15}(CO)_{27}]^{3-}$ and $[Rh_{14}(CO)_{26}]^{2-}$ [41].

Molecular hydrogen may also act as a reducing agent towards MCCs through the H^+/H_2 redox couple (reaction (2).

$$2H^+ + 2e^- \leftrightarrow H_2 \quad (2)$$

This is well exemplified by the reduction of higher nuclearity Chini clusters $[Pt_{3n}(CO)_{6n}]^{2-}$ (n = 2–10) to lower nuclearity ones, an example being the transformation of $[Pt_{12}(CO)_{24}]^{2-}$ (Pt formal oxidation state −0.167) into $[Pt_9(CO)_{18}]^{2-}$ (Pt −0.222) [42–44]. The reaction may be reversed upon addition of acids acting as oxidizing agents (reaction (3).

$$3\left[Pt_{12}(CO)_{24}\right]^{2-} + H_2 \leftrightarrow 4\left[Pt_9(CO)_{18}\right]^{2-} + 2H^+ \quad (3)$$

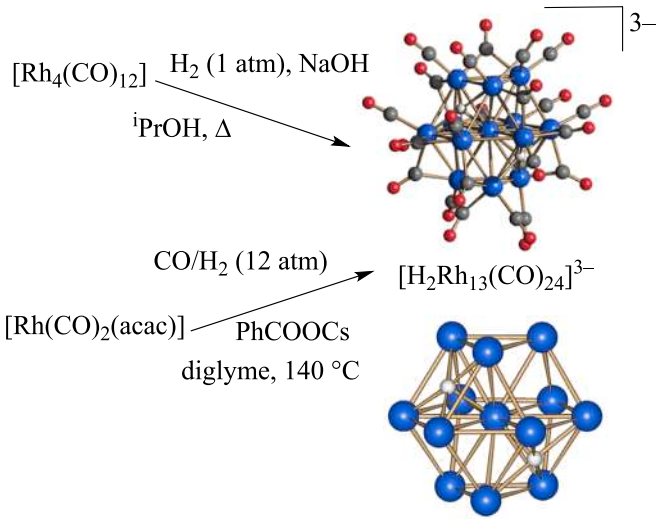

Fig. 4. Two alternative syntheses of $[H_2Rh_{13}(CO)_{24}]^{3-}$: (a) low pressure synthesis from $[Rh_4(CO)_{12}]$; (b) high pressure synthesis from $[Rh(CO)_2(acac)]$ (blue, Rh; red, O; grey, C; white, H). The cluster contains two semi-interstitial μ_5-H ligands located in square pyramidal cavities. The H_2Rh_{12} cage is outlined at the bottom of the figure.

2.2. Syntheses of hydride MCCs using proton sources

As noticed at the beginning of Section 2, hydride ligands are often added to MCCs as protons, by means of acids (entry (c) of the list), water molecules (entry (d) of the list), alcohols or other organic molecules containing weakly acidic H-atoms (entry (e) of the list). Indeed, anionic MCCs may behave as Bronstead bases and be easily protonated by H^+ donors. It must be remarked that H^+ ions may also act as oxidizing agents *via* the H^+/H_2 redox couple, in a process which is the reverse of that described at the end of Section 2.1. Overall, the reactions of MCCs with H^+ may have different outcomes:

(1) Oxidation to give a non-hydride MCC;
(2) Protonation with formation of a hydride MCC with the same nuclearity and number of CO ligands of the parent species;
(3) Oxidation and protonation to give a hydride MCC with a different nuclearity compared to the parent species.

Several examples of oxidation reactions of MCCs by means of acids are known and will not be discussed in detail [15–21,30,31,43–45]. As an example, reaction (3) may be reversed, and $[Pt_9(CO)_{18}]^{2-}$ is oxidized to $[Pt_{12}(CO)_{24}]^{2-}$ by strong acids, such as HBF_4 or H_2SO_4. The anionic species $[Fe_3(CO)_{11}]^{2-}$ is protonated to $[HFe_3(CO)_{11}]^-$ by strong acids but, further addition of acids results in its oxidation to $[Fe_3(CO)_{12}]$; overall, the oxidation state of Fe passes from −0.667 to 0. As a further example, the reaction of $[Fe_6C(CO)_{16}]^{2-}$ with H^+ ions affords $[Fe_5C(CO)_{15}]$ with overall oxidation of Fe from −0.333 to 0 [45,46]. As evidenced by these three examples, oxidation of MCCs by acids may retain, decrease or increase the nuclearity of the cluster.

Protonation of anionic MCCs to hydride MCCs is very common, and a representative example is reported in Fig. 5 [47]. Strong acids such as HBF_4, CF_3SO_3H, CF_3COOH, H_2SO_4, are used as proton sources but, depending on the basicity of the MCC anion, also weaker acids may be used, including water, alcohols and other organic molecules. For instance, $[Fe(CO)_4]^{2-}$ is protonated by CH_3CN resulting in the formation of $[HFe(CO)_4]^-$.

Anionic MCCs can often undergo multiple protonation steps, that can be reversed by treatment with bases such as NaOH, Na_2CO_3, amines (Fig. 6) [48]. Sometimes even the solvent itself may act as a base deprotonating a hydride MCC; this applies particularly to polar solvents

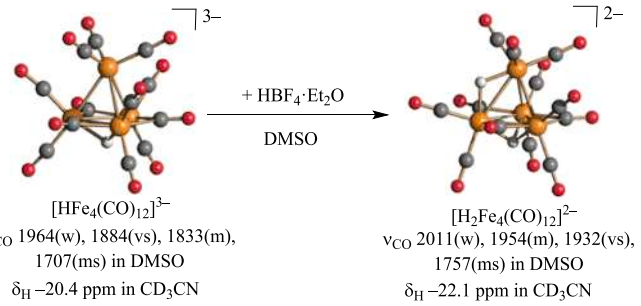

Fig. 5. Protonation of $[HFe_4(CO)_{12}]^{3-}$ (one μ_3-H) and formation of $[H_2Fe_4(CO)_{12}]^{2-}$ (one μ_3-H and one μ-H), with pertinent IR and ^1H NMR data (orange, Fe; red, O; grey, C; white, H).

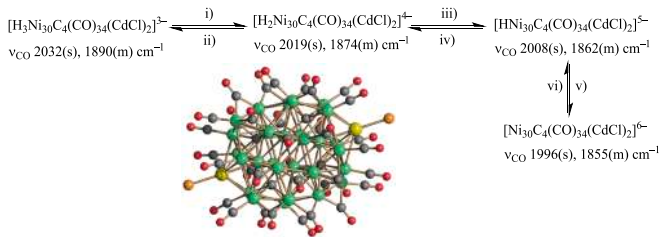

Fig. 6. Protonation/deprotonation equilibria of $[H_{6-n}Ni_{30}C_4(CO)_{34}(CdCl)_2]^{n-}$ (n = 3–6). The anions $[H_{6-n}Ni_{30}C_4(CO)_{34}(CdCl)_2]^{n-}$ (n = 4–6) are isostructural as determined by SC-XRD (hydride ligands have not been located) (green, Ni; yellow, Cd; orange, Cl; red, O; grey, C). i) Dissolution in acetone without acids. ii) + H_2SO_4 in acetone. iii) dissolution in CH_3CN. iv) + H_2SO_4 in acetone. v) + $NaHCO_3$ or 4,4′-bipyridine in CH_3CN or DMF. vi) + H_2O in in CH_3CN or DMF. Adapted from ref. [48] with permission from Wiley.

such as CH_3CN, DMF and DMSO. Reversible protonation/deprotonation reactions are, overall, very common in the case of poly-hydride MCCs (Sections 4 and 5).

The site of protonation of MCCs is usually their metal cage, unless exposed heteroatoms suitable for protonation are present. For instance, protonation of $[Fe_3O(CO)_9]^{2-}$ occurs at the O-atom affording $[Fe_3(OH)(CO)_9]^-$ [49], whereas $[HFe_3S(CO)_9]^-$ is obtained upon reaction of $[Fe_3S(CO)_9]^{2-}$ with acids (Fig. 7) [50]. Addition of one mole equivalent of H^+ to $[Fe_4C(CO)_{14}]^{2-}$ results in the hydride $[HFe_4C(CO)_4]^-$, whereas the second H^+ ion is added to carbon atom, and not to the metal cage, eventually affording $HFe_4(CH)(CO)_{14}$ [51].

Protonation of the O-atom of coordinated CO ligands is very rare and, to the best of our knowledge, not a single example has been yet

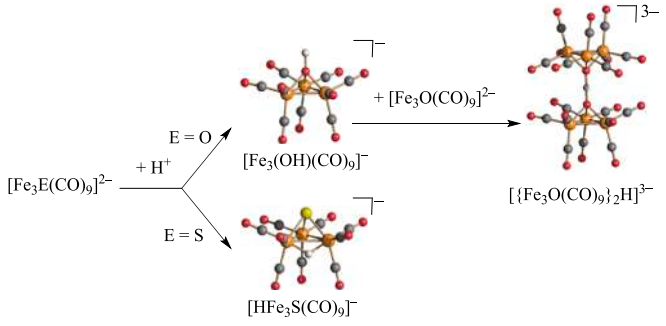

Fig. 7. Different protonation sites of $[Fe_3E(CO)_9]^{2-}$ (E = O, S) depending on the nature of the exposed heteroatom. Protonation occurs on the metal cage when E = S affording a $[HFe_3S(CO)_9]^-$ hydride species displaying one μ-H. In contrast, the $[Fe_3(OH)(CO)_9]^-$ hydroxide cluster is formed upon O-protonation. The latter species dimerizes during crystallization affording $[\{Fe_3O(CO)_9\}_2H]^{3-}$, which contains an exceptionally short O—H···O hydrogen bond (orange, Fe; yellow, S; red, O; grey, C; white, H).

reported for high nuclearity MCCs. Conversely, there is spectroscopic evidence (^{1}H and ^{13}C NMR) that $[HFe_3(CO)_{11}]^-$ and $[HFe_4(CO)_{13}]^-$ react at low temperature (−90 °C) in CD_2Cl_2 with HSO_3F affording $[HFe_3(CO)_{10}(COH)]$ and $[HFe_4(CO)_{12}(COH)]$, respectively [52,53]. These species are very unstable and decompose upon heating to room temperature, hampering their structural characterization by SC-XRD. Similarly, protonation of $[HRu_3(CO)_{11}]^-$ (δ_H –11.8 ppm) in CD_2Cl_2 with HSO_3F at −60 °C initially generates $[HRu_3(CO)_{10}(COH)]$ (δ_H –14.6 and + 16.1 ppm), but rapidly the second proton migrates from oxygen to the metal cage, and $[H_2Ru_3(CO)_{11}]$ (δ_H –12.0 and –18.7 ppm) is the only product in solution at −30 °C (Scheme 2) [54]. The latter probably contains one terminal and one edge bridging carbonyl, as $[H_2Os_3(CO)_{11}]$ [55]. Nonetheless, the Ru analogue is not stable and decomposes to $[Ru_3(CO)_{12}]$ at 25 °C with H_2 release.

In the case of $[Co_3(CO)_9(COH)]$ there is SC-XRD structural evidence that protonation occurs at the O-atom of a μ$_3$-CO ligand [56]. The neutral compound has been obtained by protonation of $Li[Co_3(CO)_{10}]$ with anhydrous HCl in toluene/*n*-hexane at −80 °C under Ar atmosphere, followed by stirring at −17 °C for 5 min, filtration at the same temperature and crystallization at −65 °C under CO atmosphere. The crystals are highly unstable and must be stored at liquid nitrogen temperature. It must be remarked that $[H_2Ru_5(CO)_{14}(\mu_4\text{-}COH)]^-$ contains a hydrogen bonded to the O-atom of CO, but this is prepared from $[Ru_3(CO)_9BH_4]^-$ and not from direct protonation [57].

As noticed above, the reaction of a MCC with acids may also results in a higher nuclearity hydride MCC upon a combination of oxidation and protonation (Fig. 8) [58].

Water is a very common source of hydride ligands in MCC chemistry. Water may be intentionally added or be present as moisture trace in the solvent (Fig. 9) [59,60], or as hydration molecule of some salts employed in the synthesis. The reactions may be performed at room temperature or higher temperature [61–63]. Hydrolysis due to metal ions may enhance the proton donor ability of water [64]. This is particularly true when salts such as $ZnCl_2$, $CdCl_2$, $InCl_3$, are employed (Fig. 10) [65].

Alcohols, like water, may be used as proton sources for the synthesis of hydride MCCs. Moreover, hydride ligands may arise also from other organic molecules, even if sometimes the mechanism might be different from protonation. For instance, Ir hydride MCCs have been generated from the thermal treatment of $Ir_4(CO)_{12}$ with Ph_3GeH, which is likely to act as a H^- transfer agent [66]. Moreover, photolysis of $Os_3(CO)_9(\mu_3\text{-}C_6H_6)$ affords $H_2Os_3(CO)_9(\mu_3\text{-}C_6H_4)$, likely *via* a radical mechanism (homolytic splitting of two C—H bonds) [67].

2.3. Syntheses of hydride MCCs involving nucleophilic attack of OH^- to CO

Formation of hydrides upon nucleophilic attack of OH^- ions to coordinated CO ligands (entry (f) of the list) is a typical reaction of metal carbonyl chemistry (Scheme 3) [17,30]. The first step of the reaction of a generic $[M_n(CO)_x]^{y-}$ cluster with OH^- is the formation of a metallacarboxylic acid $[M_n(CO)_{x\text{-}1}(COOH)]^{(y+1)-}$, that can eliminate CO_2 affording a $[HM_n(CO)_{x\text{-}1}]^{(y+1)-}$ hydride MCC. If stable, this hydride may be isolated, otherwise it can be deprotonated by further OH^- ions resulting in $[M_n(CO)_{x\text{-}1}]^{(y+2)-}$. Alternatively, $[M_n(CO)_{x\text{-}1}(COOH)]^{(y+1)-}$ may be directly deprotonated by OH^- resulting in the $[M_n(CO)_{x\text{-}1}(COO)]^{(y+2)-}$ metallacarboxylate, that may afford $[M_n(CO)_{x\text{-}1}]^{(y+2)-}$ upon CO_2 elimination. Depending on the relative stability of the other species involved, the $[HM_n(CO)_{x\text{-}1}]^{(y+1)-}$ hydride MCC may be or may be not isolated. Interestingly, the alternative formation of $[M_n(CO)_{x\text{-}1}]^{(y+2)-}$ represents the reduction of the starting $[M_n(CO)_x]^{y-}$ cluster upon replacement of one CO ligand with two electrons. Indeed, $[HM_n(CO)_{x\text{-}1}]^{(y+1)-}$ and $[M_n(CO)_{x\text{-}1}]^{(y+2)-}$ are the products usually obtained from such reactions, whereas isolation of $[M_n(CO)_{x\text{-}1}(COOH)]^{(y+1)-}$ or $[M_n(CO)_{x\text{-}1}(COO)]^{(y+2)-}$ is rarer. It must be remarked that, in some cases, $[HM_n(CO)_{x\text{-}1}]^{(y+1)-}$, $[M_n(CO)_{x\text{-}1}]^{(y+2)-}$, and the starting $[M_n(CO)_x]^{y-}$ may undergo further condensation reactions, with or without protonation/deprotonation, leading to larger $[H_aM_b(CO)_c]^{d-}$ hydrides.

This approach for the synthesis of hydride MCCs was investigated for the first time by Hieber in his seminal work on carbonylferrates and hydridocarbonylferrates (Fig. 11) [14]. More recent examples are represented by the synthesis of $[HM_4(CO)_{12}]^{3-}$ (M = Fe, Ru) upon treatment of $[HM_3(CO)_{11}]^-$ with NaOH in DMSO [68,69], or the one-pot synthesis of $[H_3Ru_4(CO)_{12}]^-$ by the reductive carbonylation of $RuCl_3$ in the presence of KOH (Scheme 4) [70]. A further example is the synthesis of $[HIr_4(CO)_9(L\text{-}L)]^-$ (L-L = diphosphine ligand) upon reaction of $[Ir_4(CO)_{10}(L\text{-}L)]$ with the base 1,8-diazabicyclo[5.4.0]undec-7-ene (DBU) in wet CH_2Cl_2 [71].

2.4. Syntheses of hydride MCCs involving hydride carbonyl complexes or modification of preformed hydride MCCs

Hydride MCCs can be synthesised using mononuclear hydride carbonyl complexes as hydride sources (*e.g.*, $[HFe(CO)_4]^-$, $[H_2Os(CO)_4]$, $[H_2Re(CO)_4]^-$) [72,73], or by modification of preformed hydride MCCs (entry (g) of the list). The reactions used to synthesize new hydride MCCs from preformed ones include reactions with CO, phosphines and other organic molecules, as well as thermal and redox reactions. Redox condensation involving two hydride MCCs, one hydride and one non-hydride MCC, or a hydride MCCs and a metal salt or complex have been often employed (Fig. 12) [74]. Moreover, addition of Lewis acids, such as $[ML]^+$ fragments (M = Cu, Ag, Au; L = phosphine or similar), to hydride MCCs is a very versatile route for the synthesis of new hydride clusters (Fig. 13) [75].

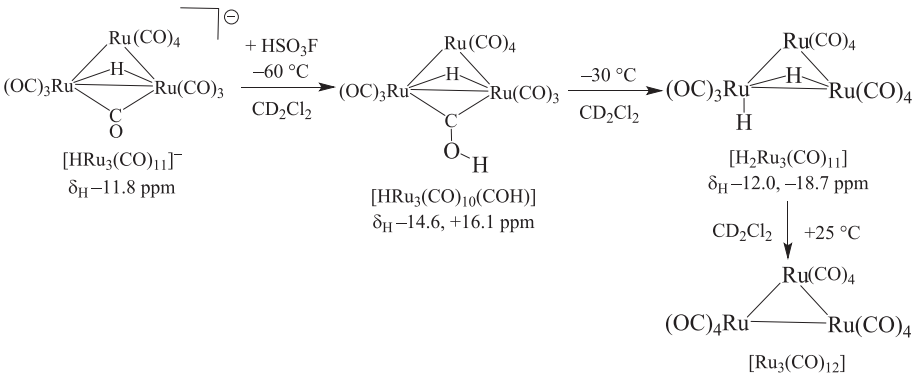

Scheme 2. Protonation of $[HRu_3(CO)_{11}]^-$ at low temperature initially occurs at the O-atom of μ-CO, followed by rapid migration to the metal cage at higher T and, eventually, decomposition to $Ru_3(CO)_{12}$.

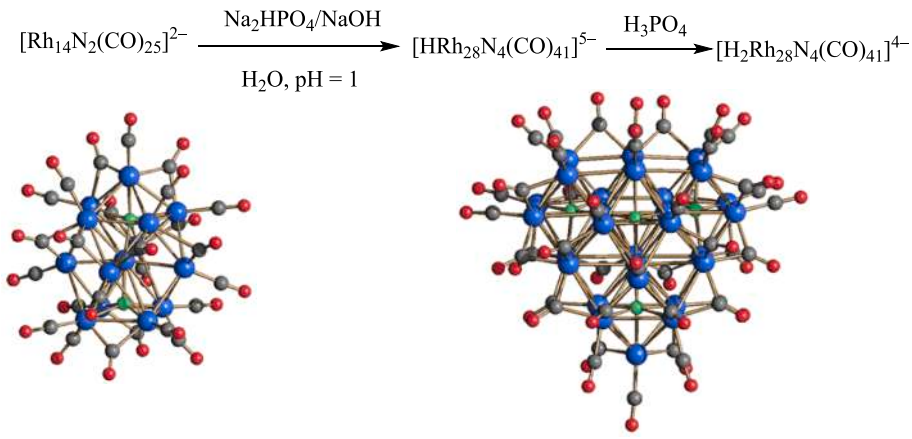

Fig. 8. Synthesis of $[HRh_{28}N_4(CO)_{41}]^{5-}$ by reaction of $[Rh_{14}N_2(CO)_{25}]^{2-}$ with acids at pH = 1. Further protonation to $[H_2Rh_{28}N_4(CO)_{41}]^{4-}$ occurs upon addition of H_3PO_4 (blue, Rh; green, N; red, O; grey, C). Hydride ligands have not been located.

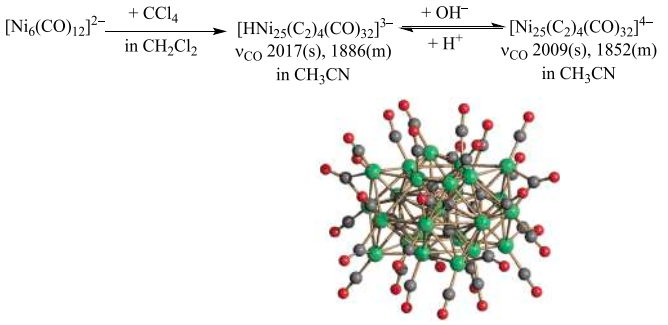

Fig. 9. $[HNi_{25}(C_2)_4(CO)_{32}]^{3-}$ is formed upon treatment of $[Ni_6(CO)_{12}]^{2-}$ with CCl_4 in CH_2Cl_2. The proton source could be moisture or the solvent. $[HNi_{25}(C_2)_4(CO)_{32}]^{3-}$ is deprotonated to $[Ni_{25}(C_2)_4(CO)_{32}]^{4-}$ by bases, such as NaOH. The reaction is reversed upon addition of acids. The molecular structures of $[HNi_{25}(C_2)_4(CO)_{32}]^{3-}$ and $[Ni_{25}(C_2)_4(CO)_{32}]^{4-}$ have been determined by SC-XRD showing almost isostructural clusters (hydride ligands have not been located) (green, Ni; red, O; grey, C). Adapted from ref. [59] with permission from The Royal Society of Chemistry.

3. Structure

The molecular structures of MCCs are usually determined by SC-XRD. The low scattering power of hydrogen atoms in X-ray diffraction poses challenges in accurately locating hydride ligands in MCCs, especially in larger clusters or when heavier atoms are present, data quality is poor, or disorder exists within the structure. In the best cases, it is possible to locate hydride ligands in the Fourier difference map and, then, refine them with or without restraints [7,76]. Alternatively, the most likely positions of hydrides can be located based on geometrical considerations, that is, elongation of M−M bonds, stereochemistry of the CO ligands, and steric requirements. This search may be supported by dedicated software such as XHYDEX [77,78], but nowadays DFT calculations are more suitable for this purpose and may be very helpful for hydride location and the general assessment of the structure of hydride MCCs. In all cases, once located, hydride ligands may be included in the SC-XRD refinement as above. Presently, the number of hydride MCCs whose structures, including location (direct or indirect) of hydride ligands, has been determined by SC-XRD is rather large, but their nuclearities do not exceed 10–13 metal atoms.

The best method for the direct location of hydride ligands would be single crystal neutron diffraction [23,79], but it requires rather large crystals. Indeed, only very few hydride MCCs have been structurally characterized by means of single crystal neutron diffraction, the most significant examples being $[HMn(CO)_5]$ [80], $[HCo_6(CO)_{15}]^-$ [25], $[HNi_{12}(CO)_{21}]^{3-}$ [26], $[H_2Ni_{12}(CO)_{21}]^{2-}$ [26], $[HRu_6(CO)_{18}]^-$ [27], $[H_2Rh_{13}(CO)_{24}]^{3-}$ [28], $[H_2Os_3(CO)_{10}]$ [81], $[H_2Os_3(CO)_{10}(\mu\text{-}CH_2)]$ [82], $[HOs_6(CO)_{18}]^-$ [83], $[H_2Os_6(CO)_{18}]$ [84], $[H_4Os_{10}(CO)_{24}]^{2-}$ [24], and $[HIr_4(CO)_{11}]^-$ [85] (Fig. 14). Even if the number of these structures is limited, they have greatly contributed to understanding the possible coordination modes of hydride ligands in MCCs. A peculiar case is represented by $[H_4Re_4(CO)_{12}]$, whose molecular structure, including hydrides, has been determined by joint SC-XRD and time-of-flight neutron

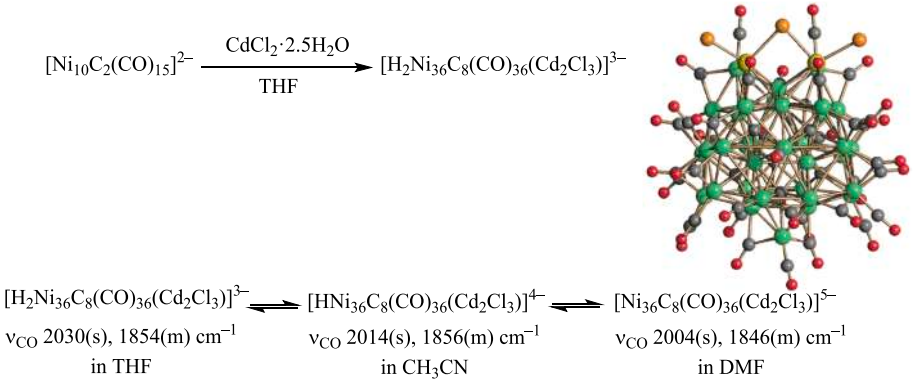

Fig. 10. Synthesis of $[H_2Ni_{36}C_8(CO)_{36}(Cd_2Cl_3)]^{3-}$ from $[Ni_{10}C_2(CO)_{15}]^{2-}$ and $CdCl_2{\cdot}2.5H_2O$ in THF. The reaction is a condensation induced by oxidation with concomitant protonation. Water is the hydride source.
The molecular structure has been determined by SC-XRD (hydride ligands have not been located) (green, Ni; yellow, Cd; orange, Cl; red, O; grey, C). Protonation/deprotonation equilibria are observed just upon dissolution in solvent of increasing polarity. Adapted with permission from Wiley from ref. [65]

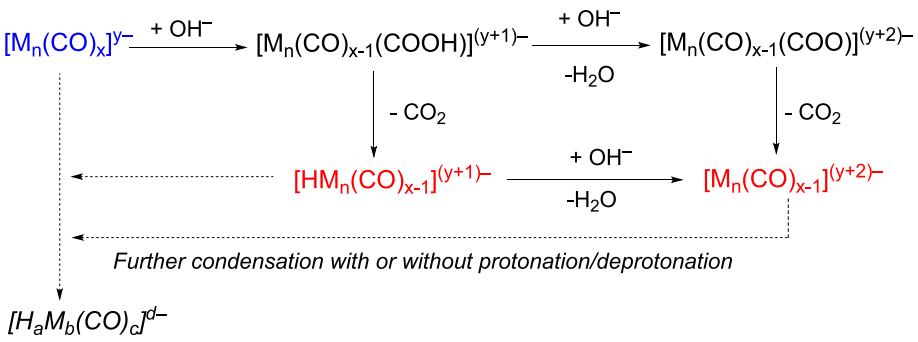

Scheme 3. Schematic representation of the reactions that can occur upon OH^- nucleophilic attack at a CO ligand of a MCC. These include the formation of an isonuclear hydride MCC, a reduced isonuclear MCC, or larger MCCs upon condensation. Metallacarboxylic acid and metallacarboxylate species are involved as intermediates, but rarely isolated.

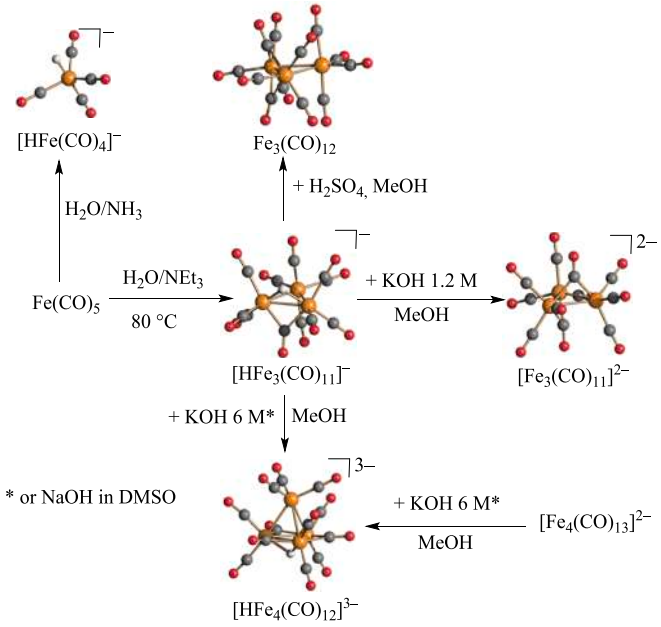

Fig. 11. $[HFe(CO)_4]^-$ (one terminal hydride) is obtained by OH^- nucleophilic attack on a CO of $Fe(CO)_5$ without further condensation. Hydroxide ions are generated by NH_3 in H_2O. Nucleophilic attack and condensation to yield $[HFe_3(CO)_{11}]^-$ (one μ-H) occur upon heating $Fe(CO)_5$ in a H_2O/Et_3N mixture. The latter is oxidized to $Fe_3(CO)_{12}$ by strong acids, whereas it is deprotonated to $[Fe_3(CO)_{11}]^{2-}$ using KOH 1.2 M in MeOH. Increasing the concentration of the base to 6 M in MeOH affords $[HFe_4(CO)_{12}]^{3-}$ (one μ_3-H). The same product can be obtained using NaOH in DMSO, or starting from $[Fe_4(CO)_{13}]^{2-}$ (orange, Fe; red, O; grey, C; white, H).

powder diffraction analysis (Fig. 15) [86]. This methodology does not require large crystals, but its application to MCCs is nowadays limited to this single example.

To the best of our knowledge, the largest MCCs, whose hydride ligands have been structurally located have a nuclearity of 10–13. Nonetheless, there is indirect spectroscopic and/or electrochemical evidence (see Sections 4 and 5) for the presence of hydrides also in larger MCCs [21,40]. The problem of locating hydrides is rather common also for other categories of clusters, and in particular ligand protected Ag and Au nanoclusters [87,88].

Based on the available structural data, hydride ligands may be found on the surface of the metal cage, or within the metal cage in interstitial or semi-interstitial positions. Some representative examples will be reported in the following discussion.

Often hydride ligands are bonded to the surface of the cluster, in terminal, edge bridging or face capping positions. Terminal hydrides are not very common in MCCs, and the few examples reported are limited to clusters with nuclearities 3–6 (Fig. 16). For instance, a single terminal hydride was found in $[HIr_4(CO)_{10}(PPh_3)]^-$ [89], $[HIr_4(CO)_9(LL)]^-$ (LL = $Ph_2PCH(Me)PPh_2$, $Ph_2P(CH_2)_2PPh_2$, $Ph_2P(CH_2)_3PPh_2$) [71], and $[HFeIr_5(CO)_{15}]^{2-}$ [90]. The clusters $[H_2Os_3(CO)_7(SnPh_2)_2(dppm)]$ (dppm = $Ph_2PCH_2PPh_2$) [91] and $[H_3Ru_3(\mu\text{-}P^tBu_2)_3(CO)_3]$ [92] contain two and three terminal hydrides, respectively, whereas

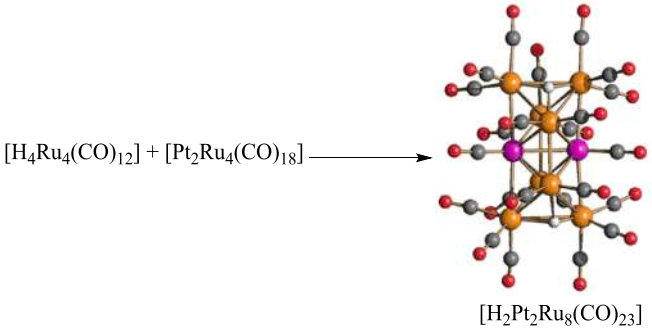

Fig. 12. $[H_2Pt_2Ru_8(CO)_{23}]$ is formed upon condensation of the $[H_4Ru_4(CO)_{12}]$ hydride MCC and the $[Pt_2Ru_4(CO)_{18}]$ non-hydride MCC. The molecular structure has been determined by SC-XRD (orange, Ru; purple, Pt; red, O; grey, C; white, H), revealing the presence of two μ_3-H ligands.

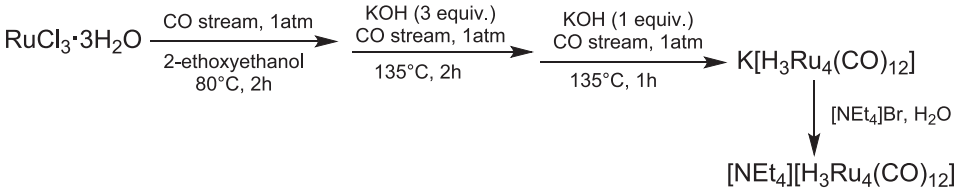

Scheme 4. One-pot synthesis of $[H_3Ru_4(CO)_{12}]^-$. The reductive carbonylation of $RuCl_3$ generates $Ru_3(CO)_{12}$ as an intermediate. This undergoes nucleophilic attack by OH^- ions which lead to formation of hydrides and condensation to the final tetranuclear cluster. Adapted from ref. [70] with permission from The Royal Society of Chemistry.

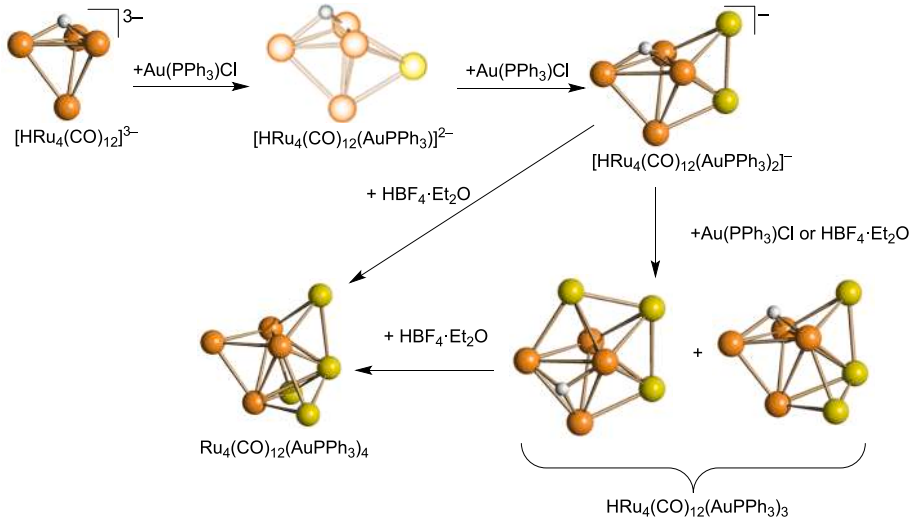

Fig. 13. Synthesis of hydride MCCs upon stepwise addition of $[AuPPh_3]^+$ fragments to $[HRu_4(CO)_{12}]^{3-}$ (orange, Ru; yellow, Au; white, H). CO and PPh_3 ligands have been omitted for clarity. Two isomers of $[HRu_4(CO)_{12}(AuPPh_3)_3]$ are obtained, which rapidly interconvert in solution. $[HRu_4(CO)_{12}(AuPPh_3)]^{2-}$ has been spectroscopically identified and its structure computationally predicted using DFT methods (lighter colors used). All other structures have been determined by SC-XRD (darker colors used). The hydride ligands are all in face-capping positions. Adapted from ref. [75] with permission from The Royal Society of Chemistry.

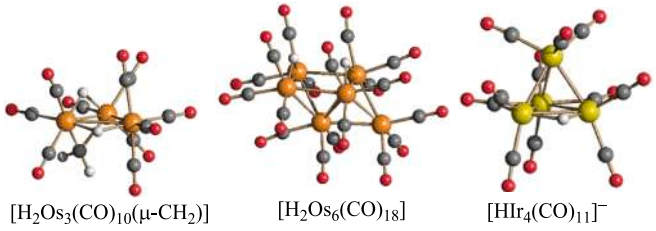

Fig. 14. Molecular structures of $[H_2Os_3(CO)_{10}(\mu\text{-}CH_2)]$, $[H_2Os_6(CO)_{18}]$, and $[HIr_4(CO)_{11}]^-$, whose edge-bridging hydride ligands have been located by single crystal neutron diffraction (orange, Ru; yellow, Ir; red, O; grey, C; white, H).

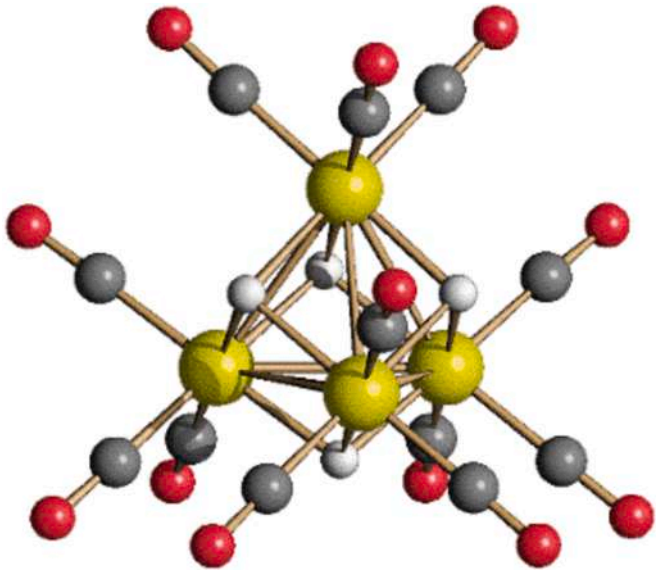

Fig. 15. The molecular structure of $[H_4Re_4(CO)_{12}]$, whose four face-capping hydride ligands have been located by a combination of SC-XRD and time-of-flight neutron powder diffraction analysis (yellow, Re; red, O; grey, C; white, H).

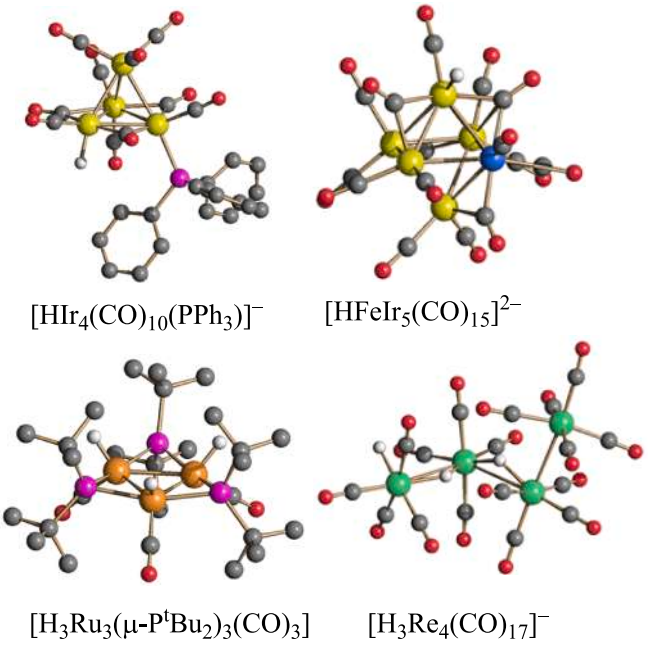

Fig. 16. Some examples of MCCs containing terminal hydrides (orange, Ru; yellow, Ir; blue, Fe; green, Re; purple, P; red, O; grey, C; white, H). H-atoms bonded to C-atoms have been omitted. $[H_3Re_4(CO)_{17}]^-$ contains one terminal and two edge-bridging hydrides, whereas all other clusters display only terminal H-ligands.

$[H_2Os_3(CO)_{10}(L)]$ (L = NH_2Et, $NHEt_2$) contains one terminal (*t*-H) and one edge bridging (μ-H) hydride [93], $[H_3Re_4(CO)_{17}]^-$ one *t*-H and two μ-H [73], $[H_8Ir_4(CO)_4(PPh_3)_4]$ four *t*-H and four μ-H [36].

Edge bridging mode is the most common coordination documented so far for hydride MCCs, which can contain from one up to eight μ-H ligands. Several examples can be found in the Figures reported in this minireview. It is noteworthy that two isomers of $[H_3Ru_4(CO)_{12}]^-$ are known, both containing three μ-H ligands, but differently arranged around the tetrahedral cage of the cluster (Fig. 17) [70,94].

Face capping hydride ligands (μ_3-H) are less common than edge bridging ones, but still rather well represented. In most cases a single μ_3-

H ligand is present, but clusters with 2–4 μ_3-H ligands are also known. For instance, $[H_4Re_4(CO)_{12}]$ displays four face capping hydrides (Fig. 15) [86]. MCCs with different hydride coordination modes have been, also, reported. For instance, $[H_4Os_{10}(CO)_{24}]^{2-}$ contains two μ-H and two μ_3-H ligands [24], whereas $[H_5Os_{10}(CO)_{24}]^-$ displays three μ-H and two μ_3-H ligands (Fig. 18) [95].

Semi-interstitial hydrides have been up to now structurally documented only in the case of $[H_2Rh_{13}(CO)_{24}]^{3-}$, which contains two μ_5-H ligands located in square pyramidal cavities (Fig. 4) [28]. The metal cage of the cluster is a Rh-centered anti-cubeoctahedron, displaying six square and eight triangular faces. Each hydride ligand is located at the center of one square face of the surface of the cluster, and additionally coordinated to the central Rh-atom. The overall H-coordination is similar to that found in semi-exposed M_5C carbide MCCs, such as $[Fe_5C(CO)_{14}]^{2-}$ [96].

Hydride ligands are located in octahedral cavities (interstitial μ_6-H) in species such as $[HCo_6(CO)_{15}]^-$ [25], $[HRu_6(CO)_{18}]^-$ [27], $[HRu_7(CO)_{19}(\mu\text{-}CNMe_2)]$ [97], $[\{HRu_6(CO)_{17}\}_2Cu_6Br_2]^{2-}$ [70], $[HNi_{12}(CO)_{21}]^{3-}$, and $[H_2Ni_{12}(CO)_{21}]^{2-}$ [26] (Fig. 19). It is noteworthy that, in $[HOs_6(CO)_{18}]^-$, the unique hydride is μ_3-H coordinated on the surface of the cluster [83], and not fully interstitial as in the Ru analogue. Similarly, multinuclear low temperature NMR studies indicate that $[HRh_6(CO)_{15}]^-$, obtained upon protonation of $[Rh_6(CO)_{15}]^{2-}$ at low temperature [98], contains a terminal hydride, and not an interstitial one as found in $[HCo_6(CO)_{15}]^-$. Unfortunately, $[HRh_6(CO)_{15}]^-$ rapidly loses H_2 at room temperature affording $[Rh_{12}(CO)_{30}]^{2-}$, hampering its full structural characterization.

The only MCC containing an interstitial μ_4-H within a tetrahedral cavity is $[HFe_4(CO)_{12}(AuPPh_3)_3]$ (Fig. 20) [99], whereas the related $[HRu_4(CO)_{12}(AuPPh_3)_3]$ exists as two exchanging isomers [75], both displaying a μ_3-H on the surface of the cluster. Due to the smaller size of Fe compared to Ru, it is likely that there is not enough space on the surface of the Fe_4 tetrahedron in order to accommodate 12 CO ligands, three $AuPPh_3$ fragments and the hydride that, therefore, moves within the tetrahedral cavity of the cluster.

A similar problem was found in the case of $[HFe_4(CO)_{13}]^-$ and $[HRu_4(CO)_{13}]^-$ [100,101]. The parent dianions $[Fe_4(CO)_{13}]^{2-}$ and $[Ru_4(CO)_{13}]^{2-}$ both possess a tetrahedral structure. This is retained upon protonation in the case of $[HRu_4(CO)_{13}]^-$, whereas $[HFe_4(CO)_{13}]^-$ displays a butterfly structure (Fig. 21). The structural rearrangement (from tetrahedron to butterfly) is promoted in the case of Fe in order to create space for the additional hydride ligand. Both the hydride migration and cage rearrangement observed in Figs. 20 and 21, respectively, are mainly sterically driven.

Reversible structural rearrangements upon protonation/deprotonation reactions have been reported also for the clusters $[H_{3-n}Co_{15}Pd_9C_3(CO)_{38}]^{n-}$ (n = 0–3) [102]. Indeed, the Pd_9 core of the cluster

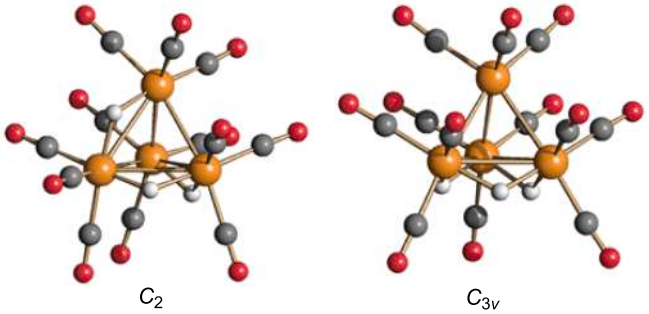

Fig. 17. Molecular structures of the C_2 and C_{3v} isomers of $[H_3Ru_4(CO)_{12}]^-$ (orange Ru; red O; grey C; white H). All hydride ligands are in edge-bridging positions. Both isomers are present in solution as shown by VT NMR experiments. Depending on the experimental conditions, the two isomers can be crystallized as separate compounds, or co-crystallized together. Adapted from ref. [70] with permission from The Royal Society of Chemistry.

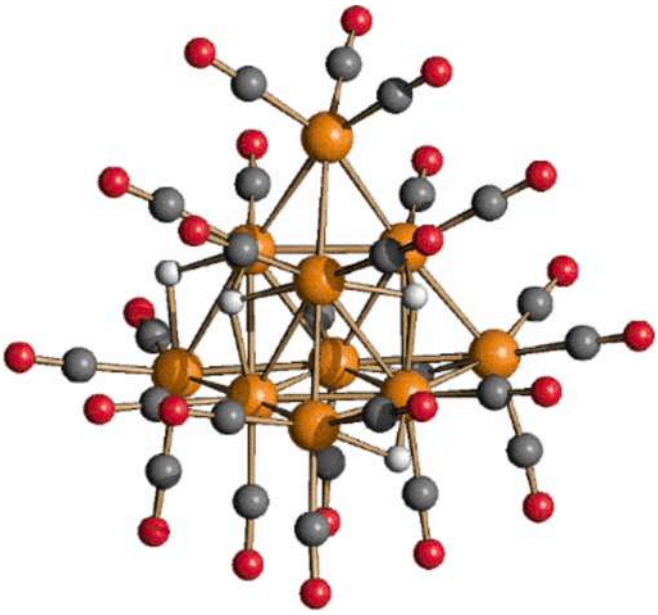

Fig. 18. Molecular structure of $[H_5Os_{10}(CO)_{24}]^-$ displaying three μ-H and two μ_3-H ligands. (orange Ru; red O; grey C; white H).

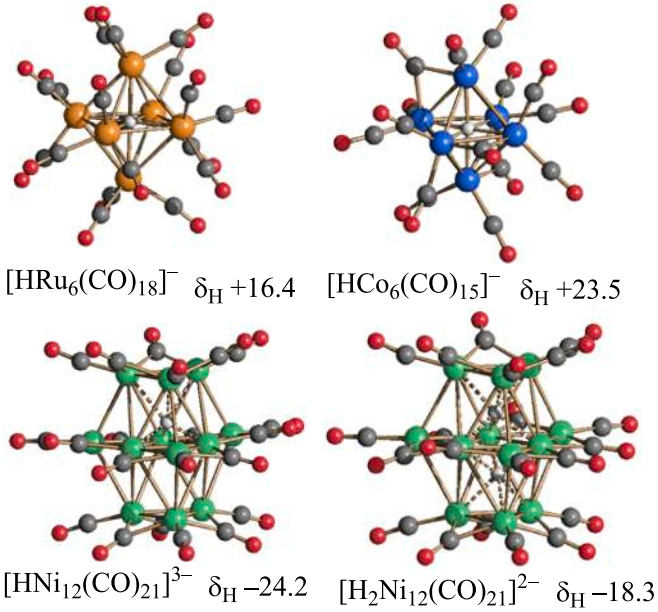

Fig. 19. Molecular structure of MCCs containing fully interstitial μ_6-H hydride ligands (orange, Ru; green, Ni; blue, Co; red, O; grey, C; white, H). Hydride ligands have been located by SC-XRD and single crystal neutron diffraction. $[HCo_6(CO)_{15}]^-$ and $[HRu_6(CO)_{18}]^-$, whose hydride are perfectly at the center of the octahedral cage, display low field resonances in their ^{1}H NMR spectra. Conversely, $[HNi_{12}(CO)_{21}]^{3-}$, and $[H_2Ni_{12}(CO)_{21}]^{2-}$, whose hydrides are significantly moved from the center of the octahedral cavities, display the usual high field resonances in their ^{1}H NMR spectra.

(Fig. 22) is a tricapped trigonal prism (TP-Pd_9) in the case of $[Co_{15}Pd_9C_3(CO)_{38}]^{3-}$, whereas it becomes a tricapped octahedron (Oh-Pd_9) in $[H_2Co_{15}Pd_9C_3(CO)_{38}]^-$ and $[H_3Co_{15}Pd_9C_3(CO)_{38}]$. Both isomers, TP-$Pd_9$ and Oh-Pd_9, have been found for the dianion $[HCo_{15}Pd_9C_3(CO)_{38}]^{2-}$ [103]. The hydride ligands have not been located in these clusters, but the observed structural rearrangements upon reaction with acids and bases may be taken as an indirect proof of the presence of the hydrides.

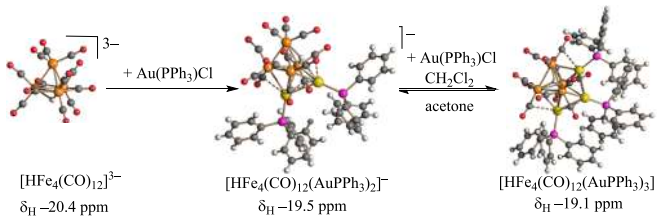

Fig. 20. Synthesis of $[HFe_4(CO)_{12}(AuPPh_3)_2]^-$ (one μ_3-H) and $[HFe_4(CO)_{12}(AuPPh_3)_3]$ (one μ_4-H) from $[HFe_4(CO)_{12}]^{3-}$ (one μ_3-H) (orange, Fe; yellow, Au; purple, P; red, O; grey, C; white, H). Neutral $[HFe_4(CO)_{12}(AuPPh_3)_3]$ is stable in CH_2Cl_2, but dissociates one $[AuPPh_3]^+$ fragment in more polar solvents, such as acetone. The process has been investigated in solution by ^1H NMR spectroscopy.

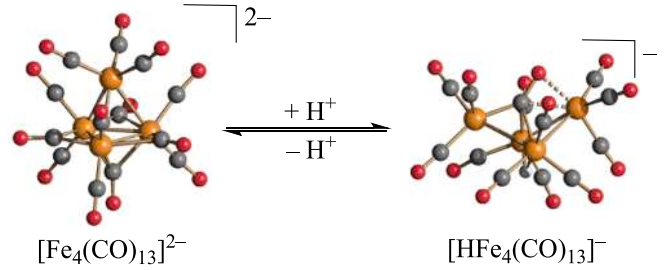

Fig. 21. Reversible structural rearrangement (tetrahedron ↔ butterfly) upon protonation/deprotonation of $[Fe_4(CO)_{13}]^{2-}$ and $[HFe_4(CO)_{13}]^-$ (one μ-H) (orange, Fe; red, O; grey, C; white, H).

To conclude this Section, it must be remarked that several larger MCCs are actually hydrides or poly-hydrides, even though the H-atoms have not been located. This problem will be further discussed in the following Sections.

4. NMR spectroscopy

^1H NMR spectroscopy is a very useful tool for studying hydride MCCs in solution, at least in the case of low to middle size clusters, that is, up to *ca.* 15–20 metal atoms. Detection of hydride resonances by ^1H NMR spectroscopy is challenging with clusters in the range 20–30 metal atoms and, to the best of our knowledge, no hydride resonance has been observed for larger hydride MCCs, regardless of the experimental conditions. The problem of detecting hydride resonances by ^1H NMR spectroscopy in larger hydride MCCs will be discussed at the end of this Section.

Surface hydrides (*t*-H, μ-H, μ_3-H) generally resonate in the range δ_H –5 to –30 ppm, making their detection rather clear also in the presence of several organic protons (Table 1) [17]. ^1H NMR data for semi-interstitial and fully interstitial hydride MCCs are far more scarce than for surface ones. The semi-interstitial hydrides (μ_5-H) of $[H_2Rh_{13}(CO)_{24}]^{3-}$ resonate at δ_H –26.7 ppm. Similar data have been reported for $[H_3Rh_{13}(CO)_{24}]^{2-}$ (δ_H –29.3 ppm) and $[HRh_{13}(CO)_{24}]^{4-}$ (δ_H –25.5 ppm) obtained upon protonation and deprotonation of $[H_2Rh_{13}(CO)_{24}]^{3-}$, respectively [39]. In the case of $[HNi_{12}(CO)_{21}]^{3-}$ and $[H_2Ni_{12}(CO)_{21}]^{2-}$, the hydride ligands are fully interstitial within distorted octahedral cavities, laying not at the center of the octahedral cavities, but closer to the inner triangular face (Fig. 19). Their hydride ligands, again, display highfield resonances at δ_H –24.2 and –18.3 ppm, respectively [104]. Interestingly, when the hydride is perfectly at the center of an octahedral cage, it displays lowfield resonances, that is, $[HCo_6(CO)_{15}]^-$ δ_H + 23.5 ppm [25], $[HRu_6(CO)_{18}]^-$ δ_H + 16.4 ppm [105], $[HRu_7(CO)_{19}(\mu\text{-}CNMe_2)]$ δ_H + 11.4 ppm [97].

Further information of the hydride environment can be obtained from homonuclear coupling to inequivalent ^1H nuclei, or heteronuclear coupling to other spin active nuclei such as ^{31}P, ^{103}Rh, ^{195}Pt and ^{13}C (upon ^{13}C-enrichment). In this sense, NMR spectroscopy may give direct evidence of the presence of hydrides in MCCs, and help understanding their structures in solution. This may be very useful to verify if the solid-state structure obtained by SC-XRD is or is not retained in solution. Indeed, in some cases, hydride MCCs can isomerize in solution, but only one isomer often crystallizes. In a few cases, it has been possible to characterize both isomers in solution by ^1H NMR spectroscopy and in the solid state by SC-XRD (see Section 3) [70,94].

Variable temperature (VT) NMR spectroscopy can be used to study dynamic processes in hydride MCCs, which may be fluxional [15–17,21,36,89,95,106].

Just as an example, $[HPt_4(CO)_4(P\hat{}P)_2]^+$ (Fig. 23) shows averaged ^1H and $^{31}P\{^1H\}$ NMR spectra at 298 K in CD_2Cl_2 solution due to fluxionality [107]. In particular, the unique hydride resonates at δ_H –2.40 ppm with time-averaged coupling to four equivalent Pt-atoms ($^{av}J_{Pt\text{-}H} = 286$ Hz) and four equivalent P-atoms ($^{av}J_{P\text{-}H} = 37$ Hz). Its $^{31}P\{^1H\}$ NMR spectrum recorded at 298 K displays a single resonance at δ_P 16.8 ppm with $^1J_{Pt\text{-}P} = 3010$ Hz, whereas the other coupling constants could not be resolved. It was not possible to freeze the ^1H and $^{31}P\{^1H\}$ NMR spectra down to 173 K. Coalescence of the $^{31}P\{^1H\}$ NMR spectrum occurs at 183 K, and two broad resonances (δ_P 6.4 and 23.4 ppm) start to appear at 173 K. Conversely, the ^1H NMR spectrum is still fluxional at 173 K. The proposed dynamic mechanism involves the migration of the hydride on the surface on the metal tetrahedron, without losing the Pt-P interactions. This should be contrasted with the proposed mechanism for the fluxionality of $[H_3Rh_{13}(CO)_{24}]^{2-}$ and $[H_2Rh_{13}(CO)_{24}]^{3-}$, where there is evidence that the hydrides migrate in the interior of the cluster, and not onto the surface [28,39]. Indeed, as the nuclearity of MCCs increases both surface and interstitial H-migrations become competitive. This high hydride mobility might be one of the causes at the origin of the problems of detecting hydride ligands by ^1H NMR spectroscopy in larger MCCs [40,45,108,109]. At the same time, this phenomenon is somehow reminiscent of the mobility of hydrogen atoms in bulk metal hydrides [29]. Indeed, porous Pd metal is used for hydrogen storage, purification and isotope separation.

Other processes occurring to hydride MCCs in solution can be unravelled by NMR spectroscopy. For instance, ^1H NMR studies of $[HFe_4(CO)_{12}(AuPPh_3)_3]$ in different solvents have demonstrated that this species is stable in CH_2Cl_2, but it dissociates one $[Au(PPh_3)]^+$ fragment in more polar solvents, such as acetone, affording $[HFe_4(CO)_{12}(AuPPh_3)_2]^-$ (Fig. 20) [99].

As noticed above, a nuclearity of 20–30 metal atoms seems to be the upper limit for the direct detection of hydride ligands in MCCs by ^1H NMR spectroscopy. Indeed, regardless of the operative conditions (concentration, solvent, temperature, spectrometer field, solution or solid-state NMR, $^1H/^2D$ replacement and solution ^2D NMR), all attempts to experimentally detect hydrides in larger MCCs by ^1H NMR spectroscopy failed. So far, the largest MCCs, that display detectable hydride resonances in the ^1H NMR spectra, are $[H_{4-n}Ni_{22}(C_2)_4(CO)_{28}(CdBr)_2]^{n-}$ (n = 2–4) [108], $[H_{8-n}Rh_{22}(CO)_{35}]^{n-}$ (n = 4, 5) [40], and $[H_xRh_{28}N_4(CO)_{41}]^{4-}$ (x likely 2) [58]. The latter tetra-nitride displays a doublet of septets at δ_H –22.8 ppm with $J_{H\text{-}Rh} = 20.7$ and 7.3 Hz in the ^1H NMR spectrum recorded at 298 K, which broadens considerably at 183 K, clearly indicating fluxionality. The related (by protonation/deprotonation reactions) poly-hydrides $[H_4Rh_{22}(CO)_{35}]^{4-}$ and $[H_3Rh_{22}(CO)_{35}]^{5-}$ show slightly broadened hydride resonances at δ_H –14.5 and –23.4 ppm, respectively (Fig. 24) [40]. These two hydride MCCs, being different chemical species, have different electrochemical behaviors, as indicated by cyclic voltammetry (CV) and differential pulse voltammetry (DPV). As it will be discussed in Section 5, electrochemical studies can be very effective to circumstantiate the presence of elusive hydride ligands in larger MCCs, when ^1H NMR spectroscopy fails.

The case of $[H_{4-n}Ni_{22}(C_2)_4(CO)_{28}(CdBr)_2]^{n-}$ (n = 2–4) seems to be very informative of the ^1H NMR behavior of hydride MCCs of increasing

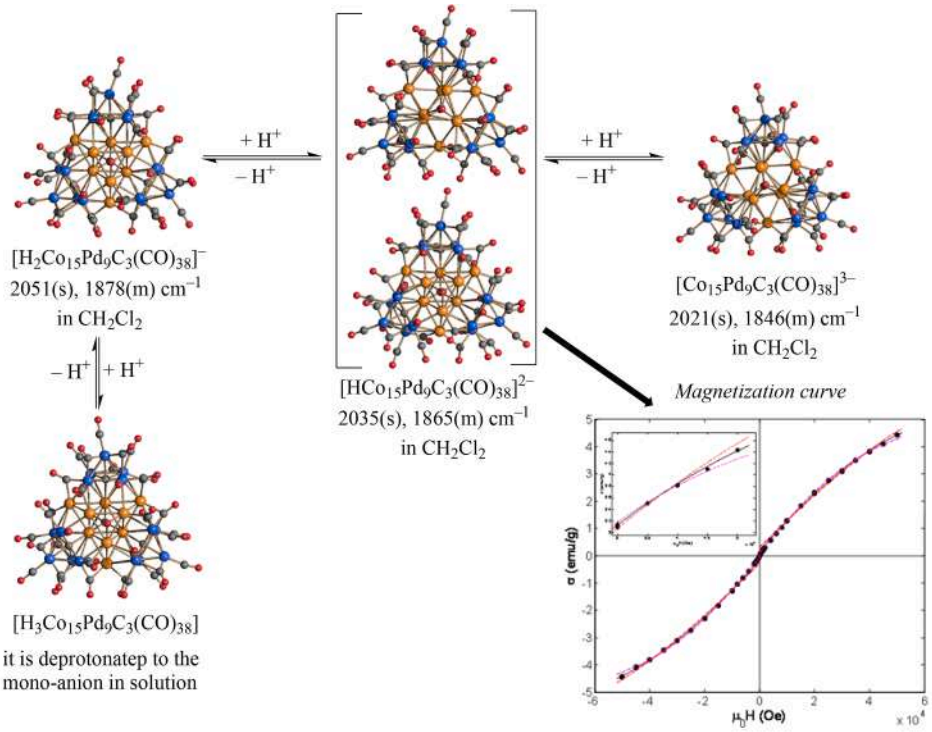

Redox changes	3–/2–	2–/1–	1–/0	0/+1
$[H_2Co_{15}Pd_9C_3(CO)_{38}]^-$	-	-	+0.104 V	+0.600 V
$[HCo_{15}Pd_9C_3(CO)_{38}]^{2-}$	-	+0.067 V	+0.398 V	+0.899 V
$[Co_{15}Pd_9C_3(CO)_{38}]^{3-}$	+0.002 V	+0.347 V	-	-

Fig. 22. Protonation/deprotonation reactions of $[H_{3-n}Co_{15}Pd_9C_3(CO)_{38}]^{n-}$ (n = 0–3) (orange, Pd; blue, Co; red, O; grey, C). Hydride ligands have not been located by SC-XRD. $[H_3Co_{15}Pd_9C_3(CO)_{38}]$ and $[H_2Co_{15}Pd_9C_3(CO)_{38}]^-$ display an Oh-Pd_9 core, whereas $[Co_{15}Pd_9C_3(CO)_{38}]^{3-}$ adopt a TP-Pd_9 structure (Oh = octahedron; TP = trigonal prism). Both isomers have been found in the case of $[HCo_{15}Pd_9C_3(CO)_{38}]^{2-}$. The graph reports the magnetization in function of field of $[NMe_3(CH_2Ph)]_2[HCo_{15}Pd_9C_3(CO)_{38}]\cdot C_6H_{14}$ as measured at 5 K (black dots). The data were fitted with the Brillouin function for different S values and Landé g-factor of free electron. Dashed lines are the best fits for S = 1/2 (red) and S = 3/2 (magenta). The black solid line represents the best-fitting curve from least-squares analysis for S = 1. Inset: zoom of the high field region. The table reports the formal electrode potentials (in V, vs. S.C.E.) for the redox changes exhibited by $[H_{3-n}Co_{15}Pd_9C_3(CO)_{38}]^{n-}$ (n = 1–3) in CH_2Cl_2. Adapted from ref. [102] with permission from The Royal Society of Chemistry.

Table 1
^{1}H NMR chemical shift ranges (ppm) for surface, semi-interstitial and interstitial hydrides bonded to MCCs. The ranges are indicative, and there might be exceptions.

Hydride coordination mode	Chemical shift range (ppm)
t-H	–5 to –20
μ-H	–5 to –25
μ_3-H	–10 to –30
μ_4-H	–19.1 [a]
μ_5-H	–5 to –25 [b]
μ_6-H (*asym*) [c]	–18 to –24
μ_6-H (*sym*) [d]	+11 to + 24

[a] The only known MCC containing a μ_4-H ligand is $[HFe_4(CO)_{12}(AuPPh_3)_3]$ [99]. [b] As found in $[HRh_{13}(CO)_{24}]^{4-}$, $[H_2Rh_{13}(CO)_{24}]^{3-}$, and $[H_3Rh_{13}(CO)_{24}]^{2-}$ [39]. [c] As found in $[HNi_{12}(CO)_{21}]^{3-}$ and $[H_2Ni_{12}(CO)_{21}]^{2-}$ [26]. The hydrides are not at the center of the octahedral cage, but closer to the inner triangular face (Fig. 19). [d] As found in $[HCo_6(CO)_{15}]^-$ δ_H + 23.5 ppm [25], $[HRu_6(CO)_{18}]^-$ δ_H + 16.4 ppm [105], $[HRu_7(CO)_{19}(\mu\text{-}CNMe_2)]$ δ_H + 11.4 ppm [97]. The hydrides are perfectly at the center of the octahedral cage.

sizes (Fig. 25) [108]. These three anions can be reversibly interconverted by protonation/deprotonation reactions, and the processes spectroscopically identified by IR and ^{1}H NMR. Broad hydride resonances have been detected for $[H_2Ni_{22}(C_2)_4(CO)_{28}(CdBr)_2]^{2-}$ (δ_H –14 ppm) and $[HNi_{22}(C_2)_4(CO)_{28}(CdBr)_2]^{3-}$ (δ_H –30 ppm), whereas $[Ni_{22}(C_2)_4(CO)_{28}(CdBr)_2]^{4-}$ does not show any hydride resonance. VT ^{1}H NMR studies of $[H_2Ni_{22}(C_2)_4(CO)_{28}(CdBr)_2]^{2-}$ and $[HNi_{22}(C_2)_4(CO)_{28}(CdBr)_2]^{3-}$ suggest the occurrence of complex dynamic exchange processes in solution, and a surprising temperature dependence of the chemical shift, that is, a drift *ca.* 0.2 ppm K^{-1} rather than *ca.* 0.05 ppm K^{-1} as in other hydride MCCs.

Further increasing the nuclearity of the clusters, the hydride resonances become so broad to be lost in the baseline of the spectrum. This phenomenon depends also on the involved metals and, for instance, it seems less marked for Rh compared to Ni. Nonetheless, based on the experimental evidence, above a nuclearity of 30 metal atoms, all hydride MCCs seems to be silent in the ^{1}H NMR spectra, regardless the nature of the metal atoms. In these cases, indirect methods can be used in order to support the hydride nature of such species, as it will be discussed in Section 5.

A theoretical explanation supporting this experimental evidence is not yet available, but it might be that the problems of detecting hydrides by ^{1}H NMR spectroscopy in larger MCCs originate from a combination of different factors, including the following:

(a) Solubility and concentration issues. Owing the high molecular weights of larger hydride MCCs, the actual concentration of hydride atoms is very low.

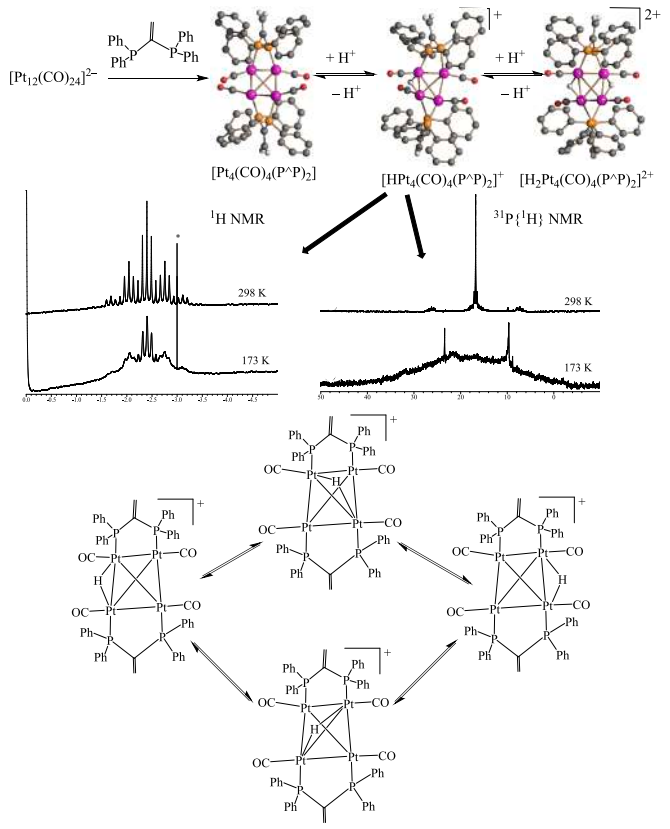

Fig. 23. Synthesis, molecular structures and protonation/deprotonation reactions of $[H_nPt_4(CO)_4(P\hat{}P)_2]^{n+}$ (n = 0–2; P^P = $CH_2 = C(PPh_2)_2$) (purple, Pt; orange, P; red, O; grey, C; white, H). Hydride ligands are all located in edge-bridging positions as determined by SC-XRD. The mono-cation mono-hydride $[HPt_4(CO)_4(P\hat{}P)_2]^+$ is fluxional in solution as shown by VT ^1H and $^{31}P\{^1H\}$ NMR studies in CD_2Cl_2 solution. The proposed migration mechanism involves the movement of the hydride ligand from one edge to the other of the tetrahedron without losing the Pt-P interaction. Adapted with permission from ref. [107] Copyright 2013 American Chemical Society.

(b) Isomerization, dynamic site-exchange processes and fluxionality. Several sites are available in larger clusters for hydride coordination, and the presence of several isomers is very likely. Fast exchange pathways may be possible on the surface of the clusters or through their metal cages, that increase by increasing the cluster size.
(c) Relaxation. Very short or very long relaxation times may make hydride detection more difficult.
(d) Aggregation phenomena in solution. Formation of large aggregates in solution may affect the NMR behaviour of the clusters. There is some DLS evidence for the formation of MCC aggregates in solution [44,110,111].
(e) Incipient metallisation of the metal core of MCCs is expected as their nuclearity increases, as also documented by electrochemical studies (see Section 5). This should cause the onset of magnetic properties in the ground and/or excited states of larger MCCs. Indeed, SQUID and EPR measurements have unequivocally demonstrated that also even electrons MCCs may be paramagnetic [102,112].

5. Electrochemistry

5.1. Electrochemistry as an indirect tool for determining the hydride nature of large MCCs

As evidenced in Section 4, the detection of hydride ligands by ^1H NMR spectroscopy fails as their nuclearity increases. Moreover, as reported in Section 3, direct location of hydrogen atoms by SC-XRD in large clusters is not possible. At this point, only indirect proofs of the hydride nature of larger MCCs can be obtained, based on a combination of IR spectroscopy, SC-XRD analyses, electrochemical and spectroelectrochemical methods [40,113,114]. The procedure adopted for assessing the hydride nature of larger MCCs can be summarized as follow:

1) Protonation/deprotonation of the cluster is studied in solution by IR spectroscopy, using solvents of increasing polarity as well as reactions with acids and bases. The anionic charge of the cluster decreases by one unit upon protonation, and increases by one unit upon deprotonation. The change of the anionic charge is clearly evidenced by the shift of the ν_{CO} bands of the cluster in the IR spectrum.
2) The fact that a MCC retain the same structure upon protonation/deprotonation, but its charge changes, can be further assessed by SC-XRD, if single crystals are obtained. Even if it is almost impossible to locate hydrides by SC-XRD in larger MCCs, their charge can be easily determined by counting the counter-ions.
3) The electrochemical behavior of isostructural but differently charged MCCs obtained by protonation/deprotonation is investigated by cyclic voltammetry (CV), differential pulse voltammetry (DPV) and/or IR spectroelectrochemistry (IR *SEC*).
4) If two isostructural MCCs with different charges exhibit the same redox properties, it suggests that they represent the same chemical species differing only in their oxidation state due to the addition or removal of one electron. Thus, the charge of the MCC changes due to redox processes. In this case, the reaction with acids does not result in protonation of the cluster, but oxidation via the H^+/H_2 redox couple.
5) If two isostructural MCCs with different charges have different redox properties, it means that they are different compounds. The only difference can be the presence/absence of one H-atom, since all other atoms are located by SC-XRD.
6) In the case of poly-hydride MCCs, this procedure should be applied to all the species involved.

This procedure has been directly assessed in the case of $[H_4Rh_{22}(CO)_{35}]^{4-}$ and $[H_3Rh_{22}(CO)_{35}]^{5-}$, for which there is still ^1H NMR evidence of their hydride nature (Fig. 24) [40]. As mentioned in Section 4, indeed these two species have different CV and DPV profiles.

A further proof of this approach is given by $[H_{3-n}Co_{15}Pd_9C_3(CO)_{38}]^{n-}$ (n = 0–3), whose structures have been described in Section 3 (Fig. 22) [102]. Also in this case, the different species can be reversibly interconverted by protonation/deprotonation with acids and bases. The neutral cluster $[H_3Co_{15}Pd_9C_3(CO)_{38}]$ is deprotonated to $[H_2Co_{15}Pd_9C_3(CO)_{38}]^-$ upon dissolution in any organic solvent and, thus, its electrochemical behavior has not been studied. Conversely, the three anionic clusters $[H_{3-n}Co_{15}Pd_9C_3(CO)_{38}]^{n-}$ (n = 1–3) show different CV profiles. Moreover, SQUID measurements at 5 K on crystals of $[HCo_{15}Pd_9C_3(CO)_{38}]^{2-}$ reveal a S = 1 ground-state. The fact that it is paramagnetic with two unpaired electrons clearly indicates that the dianion possesses an even number of electrons, which can be explained only assuming the presence of one hydride. It must be also remarked that $[H_2Co_{15}Pd_9C_3(CO)_{38}]^-$ does not show any electrochemical reduction process and, thus, formation of the dianion cannot be a reduction but it must be a deprotonation. The same applies to $[HCo_{15}Pd_9C_3(CO)_{38}]^{2-}$, which can be electrochemically oxidized but not reduced.

The electrochemical studies on $[H_{8-n}Rh_{22}(CO)_{35}]^{n-}$ (n = 4, 5) and $[H_{3-n}Co_{15}Pd_9C_3(CO)_{38}]^{n-}$ (n = 1–3), beside corroborating their hydride nature, show that they undergo several reversible redox processes [40,102]. This confirms the propensity of larger MCCs to behave as electron-sink and molecular nanocapacitors (See Section 5.2) [113–120].

As a further example, $[H_2Ni_{30}C_4(CO)_{34}\{Cu(CH_3CN)\}_2]^{4-}$ can be prepared from $[Ni_9C(CO)_{17}]^{2-}$ and $[Cu(CH_3CN)_4][BF_4]$ in THF (Fig. 26)

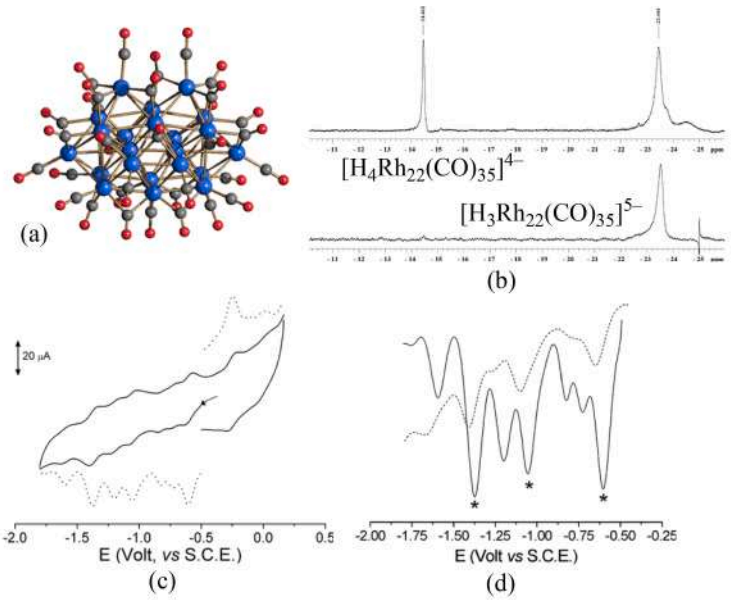

Compound	Reduction				Oxidations		Solvent
$[H_3Rh_{22}(CO)_{35}]^{5-}$	−1.59	−1.41	−1.10	−0.65	−0.24	+0.18	DMF
$[H_3Rh_{22}(CO)_{35}]^{5-}$	−1.60	−1.38	−1.05	−0.60	−0.24		CH_3CN
$[H_4Rh_{22}(CO)_{35}]^{4-}$		−1.20	−0.82	−0.73	+0.01		CH_3CN

Fig. 24. (a) Molecular structure of $[H_{8-n}Rh_{22}(CO)_{35}]^{n-}$ (n = 4, 5) (blue, Rh; red, O; grey, C). Hydride ligands have not been located by SC-XRD. (b) ^{1}H NMR spectra of (upper trace) a mixture of $[H_4Rh_{22}(CO)_{35}]^{4-}$ (δ_H −14.5 ppm) and $[H_3Rh_{22}(CO)_{35}]^{5-}$ (δ_H −23.4 ppm) in CD_3CN, and (lower trace) $[H_3Rh_{22}(CO)_{35}]^{5-}$ in d_6-DMSO. (c) CV (full line) and DPV (dotted line) of a mixture of $[H_4Rh_{22}(CO)_{35}]^{4-}$ and $[H_3Rh_{22}(CO)_{35}]^{5-}$ in CH_3CN. (d) Comparison between the DPV profiles of the mixture of the two clusters in CH_3CN (full line) and pure $[H_3Rh_{22}(CO)_{35}]^{5-}$ in DMF. The Table reports the formal redox potentials (in V, vs SCE) of the reversible redox processes of $[H_{8-n}Rh_{22}(CO)_{35}]^{n-}$ (n = 4, 5). Adapted with permission from ref. [40] Copyright 2011 American Chemical Society.

[121]. As an indirect proof of its hydride nature, it undergoes reversible protonation/deprotonation reactions, by means of HBF_4 and NaOH, leading to the formation of the four species $[H_{6-n}Ni_{30}C_4(CO)_{34}\{Cu(CH_3CN)\}_2]^{n-}$ (n = 3–6), as revealed by IR spectroscopy. The anions $[H_{6-n}Ni_{30}C_4(CO)_{34}\{Cu(CH_3CN)\}_2]^{n-}$ (n = 4–6) have been electrochemically investigated, displaying rather different redox properties. For instance, $[HNi_{30}C_4(CO)_{34}\{Cu(CH_3CN)\}_2]^{5-}$ can be electrochemically reduced but not oxidized, leading to the conclusion that the related tetra- and tri-anions are formed by acid/base and not redox reactions.

Even if the procedure herein described for the assessment of the hydride nature of larger MCCs has been usually applied to species showing reversible redox processes in CV (this is rather common for larger MCCs), the same electrochemical approach can be used also when only irreversible processes are detected by CV. Indeed, even if two differently charged MCCs display different irreversible redox processes, this means that they are different chemical compounds and, thus, all the considerations reported above are still valid. Moreover, the absence of any electrochemically detectable reversible redox process is, itself, a proof of the fact that the charge changes observed upon reactions of MCCs with acids or bases is due to reversible protonation/deprotonation and not oxidation/reduction. Just as an example, the two clusters $[Ni_{36}Co_8C_8(CO)_{48}]^{6-}$ and $[HNi_{36}Co_8C_8(CO)_{48}]^{5-}$ can be reversibly interconverted using $HBF_4{\cdot}Et_2O$ and $[NBu_4][OH]$ (Fig. 27) [122]. Both these clusters display only complicated irreversible redox processes in their CVs and, in particular, $[HNi_{36}Co_8C_8(CO)_{48}]^{5-}$ shows only irreversible oxidation processes. This clearly indicates that the penta-anion cannot be converted into the *hexa*-anion by reduction, lending a further support to its hydride nature.

To conclude this Section, $[Ru_6C(CO)_{15}]^{4-}$ and $[HRu_6C(CO)_{15}]^{3-}$ are a further example of MCCs that can be reversibly interconverted by reactions with acids and bases [123]. The addition or removal of a single proton leads to distinct electrochemical properties, as evidenced by CV and IR *SEC* measurements. Since their nuclearity is low, it has been possible to directly detect the hydride of $[HRu_6C(CO)_{15}]^{3-}$ by ^{1}H NMR spectroscopy and SC-XRD.

5.2. Tuning the redox potentials of MCCs by protonation/deprotonation reactions

As pointed out in Section 5.2, larger MCCs are often multivalent, in the sense that they display two or more reversible redox processes, as clearly indicated by electrochemical investigation. Multivalent MCCs can be viewed as electron sinks and, due to their nanometric sizes and the presence of an insulating CO shell on the surface, behave as molecular nanocapacitors. Indeed, their nanometric metal core can be reversibly charged and discharged at well-defined potentials, just by adding/removing one electron each time. This topic has been reviewed by Longoni *et al.* [115], and several examples of non-hydride multivalent MCCs are known. Some representative examples are $[Ni_{32}C_6(CO)_{36}]^{6-}$ [124], $[Pt_{19}(CO)_{22}]^{4-}$ [125], $[Pt_{24}(CO)_{30}]^{2-}$ [125], $[Pt_{27}(CO)_{31}]^{4-}$ [118], $[Pt_{33}(CO)_{38}]^{2-}$ [117], $[Pt_{40}(CO)_{40}]^{6-}$ [117], $[Ni_{22-x}Pd_{20+x}(CO)_{48}]^{6-}$ (x = 0.62) [116], $[Ni_{29-x}Pd_{6+x}(CO)_{42}]^{6-}$ (x = 0.09) [116], $[Ni_{29+x}Pd_{6-x}(CO)_{42}]^{6-}$ (x = 0.27) [116], $[Rh_{21}Sb_2(CO)_{38}]^{5-}$ [126], $[Rh_{12}E(CO)_{27}]^{n-}$ (n = 4, E = Ge, Sn; n = 3, E = Bi) [127].

Multivalence is well-represented also among high nuclearity hydride MCCs and, as outlined in Section 5.1, their electrochemical investigation has been used in order to circumstantiate their hydride nature. In addition, protonation/deprotonation reactions represent a tool for the modulation of the electrochemical properties of MCCs by tuning their redox potentials (Table 2) [115]. First of all, both $E^{\circ\prime}$ and $\Delta E^{\circ\prime}$ between consecutive redox couples display small variations upon protonation/deprotonation. More importantly, the hydride derivatives require a

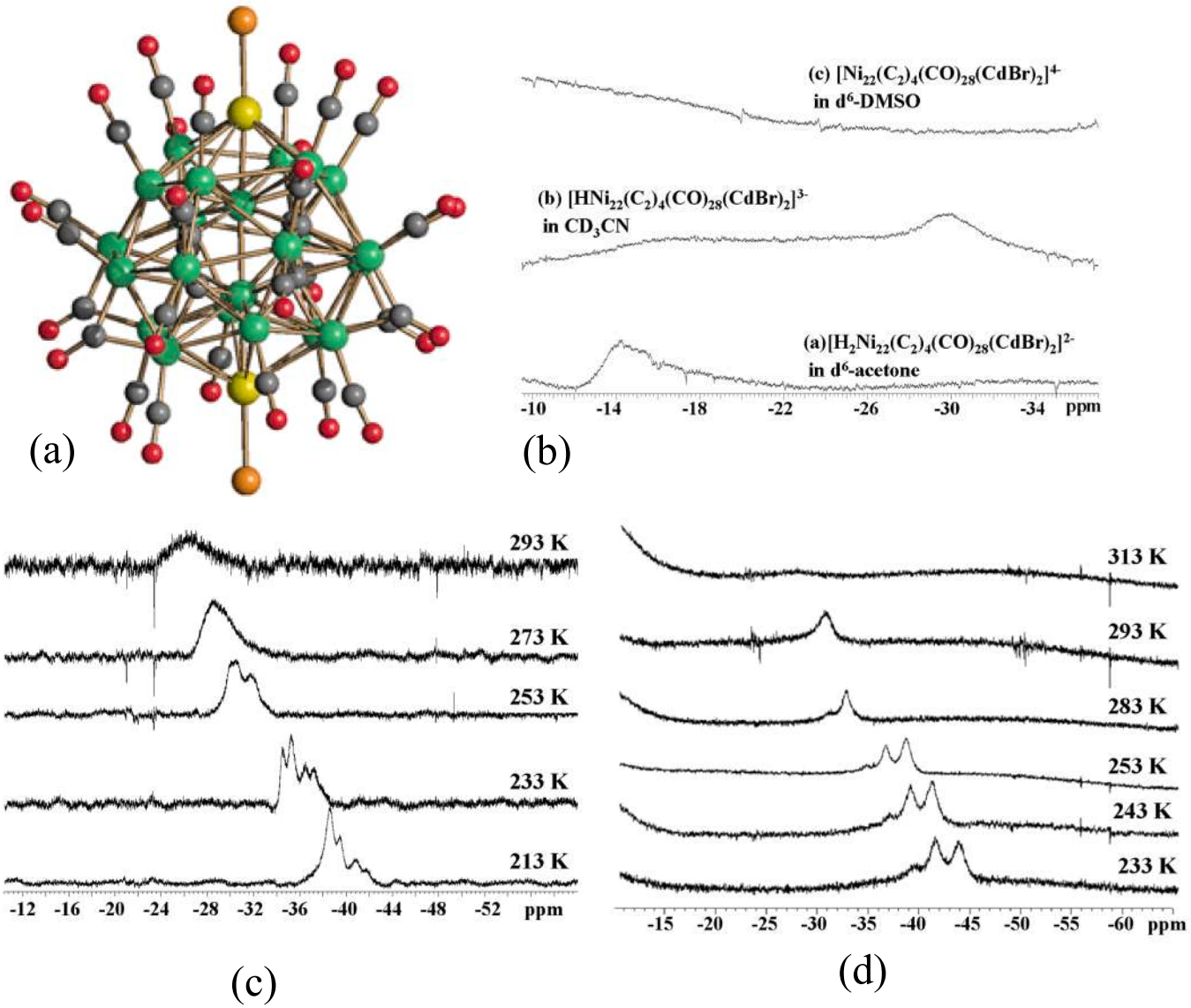

Fig. 25. (a) Molecular structure of $[H_{4-n}Ni_{22}(C_2)_4(CO)_{28}(CdBr)_2]^{n-}$ (n = 2–4) (green, Ni; yellow, Cd; orange, Br; red, O; grey, C). Hydride ligands have not been located by SC-XRD. (b) ^{1}H NMR spectra (400 MHz) recorded at 298 K in solvents of different basicity. (c) Variable temperature ^{1}H NMR spectra recorded at 600 MHz of $[HNi_{22}(C_2)_4(CO)_{28}(CdBr)_2]^{3-}$ in CD_3CN. (d) Variable temperature ^{1}H NMR spectra recorded at 600 MHz of $[HNi_{22}(C_2)_4(CO)_{28}(CdBr)_2]^{3-}$ in CD_3COCD_3. Adapted from ref. [108] with permission from The Royal Society of Chemistry.

more negative potential for the same redox change, see for instance, $[HNi_{36}Pt_4(CO)_{45}]^{5-}$ and $[Ni_{36}Pt_4(CO)_{45}]^{6-}$ [128], $[HNi_{35}Pt_9(CO)_{48}]^{5-}$ and $[Ni_{35}Pt_9(CO)_{48}]^{6-}$ [129], $[HNi_{38}Pt_6(CO)_{48}]^{5-}$ and $[Ni_{38}Pt_6(CO)_{48}]^{6-}$ [130], $[HNi_{38}C_6(CO)_{42}]^{5-}$ and $[Ni_{38}C_6(CO)_{42}]^{6-}$ [124]. This is probably because hydride and non-hydride derivatives with the same negative charge are not isoelectronic, having the hydride one additional CVE. Moreover, being electron richer, hydride MCCs often display a decreased number of reductions and an increased number of oxidation steps compared to non-hydride analogues. A similar trend is observed by further increasing the number of hydride ligands, even though a poly-hydride nature might be sometimes detrimental for electron-sink behavior. Indeed, $[H_2Ni_{38}Pt_6(CO)_{48}]^{4-}$, $[H_2Rh_{13}(CO)_{24}]^{3-}$, and $[H_3Rh_{13}(CO)_{24}]^{2-}$ show a limited number of redox processes with features of electrochemical reversibility, probably because of H_2 reductive elimination [115]. Similar considerations apply to $[H_{3-n}Co_{15}Pd_9C_3(CO)_{38}]^{n-}$ (n = 1–3) [102] and $[H_{6-n}Ni_{30}C_4(CO)_{34}\{Cu(CH_3CN)\}_2]^{n-}$ (n = 3–6) [121] described in the previous Sections.

A peculiar case is represented by $[Rh_{14}(CO)_{25}]^{4-}$ and $[HRh_{14}(CO)_{25}]^{3-}$. The non-hydride cluster does not show any reversible redox process in its CV, whereas the hydride displays two oxidations and two reductions all reversible in the timescale of CV [115]. In this case, protonation induces redox aptitude in the redox inactive $[Rh_{14}(CO)_{25}]^{4-}$.

6. Catalysis and electrocatalysis

Catalysis and electrocatalysis by MCCs have been recently reviewed and, herein, only the involvement of hydride species will be briefly discussed [30]. Indeed, several catalytic processes are known, where hydride MCCs are involved as catalyst precursors, catalytic active species, or catalytic intermediates [1,5,6,9,11,30]. The major problem of cluster catalysis is whether a MCC is the actual active species, or fragmentation to mononuclear species occurs, or catalysis is due to colloids generated from cluster decomposition. Different criteria have been elaborated to assess genuine cluster catalysis, and the reader may find pertinent readings in the references [131–135].

Two major catalytic processes, that is, hydrogenation and hydroformylation, utilize H_2 as reagent and proceed via hydride species. There

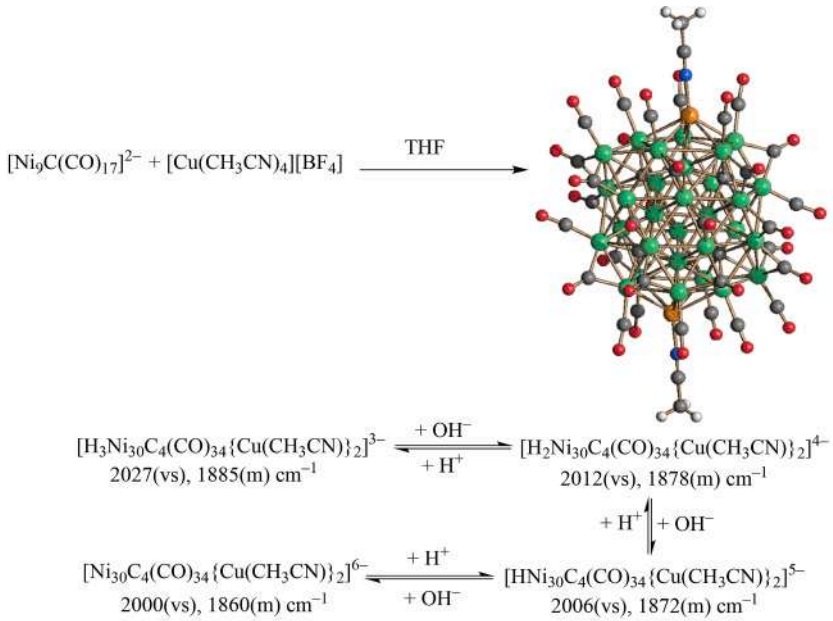

Compound	3–/4–	4–/5–	5–/6–	6–/7–	7–/8–	8–/9–	Solvent
$[H_2Ni_{30}C_4(CO)_{34}\{Cu(CH_3CN)\}_2]^{4-}$	–0.29	–0.55	–0.79	–0.98		-	Acetone
$[HNi_{30}C_4(CO)_{34}\{Cu(CH_3CN)\}_2]^{5-}$	-	-	–0.62	–1.04	–1.40	-	CH_3CN
$[Ni_{30}C_4(CO)_{34}\{Cu(CH_3CN)\}_2]^{6-}$	-	-	–0.45	–0.83	–1.03	–1.44	dmf

Fig. 26. $[H_2Ni_{30}C_4(CO)_{34}\{Cu(CH_3CN)\}_2]^{4-}$ is formed upon treatment of $[Ni_9C(CO)_{17}]^{2-}$ with $[Cu(CH_3CN)_4][BF_4]$ in THF. The proton source could be moisture or the solvent. The molecular structure has been determined by SC-XRD (hydride ligands have not been located) (green, Ni; orange, Cu; blue, N; red, O; grey, C; white, H). Reversible protonation/deprotonation reactions have been investigated by IR spectroscopy showing the formation of the four clusters $[H_{6-n}Ni_{30}C_4(CO)_{34}\{Cu(CH_3CN)\}_2]^{n-}$ (n = 3–6). The Table reports the formal redox potentials (in V, vs SCE) of the reversible redox processes of $[H_{6-n}Ni_{30}C_4(CO)_{34}\{Cu(CH_3CN)\}_2]^{n-}$ (n = 4–6). Adapted from ref. [121] with permission from The Royal Society of Chemistry.

are also several examples where hydride MCCs, directly introduced in the catalytic environment or generated *in situ* from a non-hydride MCC, are employed as homogeneous catalysts in hydrogenation and hydroformylation [30,136–152]. Hydride MCCs are also involved in other homogenous catalytic processes concerning hydrogen activation, such as water gas shift (WGS), dehydration, hydrosilylation, and ammonia borane dehydrogenation [30,136,139–141]. Some representative examples of catalytic processes using preformed hydride MCCs as catalysts, or involving hydride MCCs generated *in situ* from non-hydride MCCs, are reported in Tables 3 and 4. Further details may be found in the cited literature [137–158].

Hydride MCCs may be directly employed in homogeneous catalysis, or may be generated prior or within the catalytic cycle from a MCC precursor through the reactions described in Section 2. Molecular hydrogen is the hydride source when H_2 is employed, otherwise hydrides may arise from organic reagents or water. For instance, WGS reaction catalyzed by MCCs is likely to proceed *via* the generation of a hydride MCC through nucleophilic attack of OH^- to a coordinated CO (Scheme 5).

MCCs bearing chiral phosphines are particularly interesting for asymmetric hydrogenation. For instance, derivatives of $[Ru_3(CO)_{12}]$, $[H_4Ru_4(CO)_{12}]$ and $[H_2Ru_3S(CO)_9]$ with chiral diphosphine ligands have been used for the asymmetric hydrogenation of ketones and α,β-unsaturated carboxylic acids [148–152]. Chiral hydride MCCs, such as $[H_2Ru_3S(CO)_7(PP)]$, $[H_4Ru_4(CO)_{10}(PP)]$, and $[H_4Ru_4(CO)_{11}(P)]$, where P and PP are chiral monodentate or bidentate phosphine ligands, are used as catalysts or catalyst precursors. These catalysts operate under relatively mild conditions, typically 100 °C and 50 bar of H_2 in a 1:1 EtOH/toluene mixture, with 7–100 % conversions and 7–92 % of enantiomeric excess. Catalysis by intact clusters has been proved experimentally, and the catalytic cycle based on hydride MCCs computationally determined (Scheme 6) [149,150].

In an electrocatalytic process, energy is added at room temperature using an external applied potential, limiting MCC decomposition, at difference from homogeneous catalysis that usually employs higher temperatures. Berben *et al.* have conducted extensive research on MCC electrocatalysis [30], exploring both lower nuclearity species like $[Fe_4C(CO)_{12}]^{2-}$ and $[Fe_4N(CO)_{12}]^-$, as well as larger clusters like $[Co_{13}C_2(CO)_{24}]^{4-}$ [159–164]. MCCs have been employed as electrocatalysts in reduction reactions, that is, hydrogen evolution reaction (HER) and CO_2 reduction reaction (CO_2RR) (Table 5) [159–170].

Typically, the electrocatalytic reduction reaction mediated by a $[M_x(CO)_y]^n$ cluster is initiated by an electron transfer (ET) as the potential is applied, affording a reduced $[M_x(CO)_y]^{n-1}$ species (Scheme 7) [30]. This electrochemical elementary step is conventionally abbreviated as "E". In the case of HER, the second step is a chemical reaction (abbreviated as "C"), which is actually a proton transfer (PT) leading to $[HM_x(CO)_y]^n$. Formation of this key hydride intermediate requires that $[M_x(CO)_y]^{n-1}$ is sufficiently stable and, at the same time, enough reactive for further PT. Two different pathways are, then, possible, labelled ECEC and ECCE, respectively. In the ECEC pathway, $[HM_x(CO)_y]^n$ undergoes to a second ET resulting in the reduced hydride $[HM_x(CO)_y]^{n-1}$, followed to a second PT that recreates the starting $[M_x(CO)_y]^n$ with concomitant release of H_2. Alternatively, ECCE pathway, $[HM_x(CO)_y]^n$ is transformed into $[H_2M_x(CO)_y]^{n+1}$ *via* a second PT, followed by a second ET restoring $[M_x(CO)_y]^n$ and releasing H_2. Similar considerations apply to CO_2 reduction, the only difference being that the substrate of the second chemical reaction is CO_2 and not a second proton (Scheme 8).

The formation and stability of the hydride intermediate is fundamental for electrocatalysis by MCCs. At the same time, the intermediate

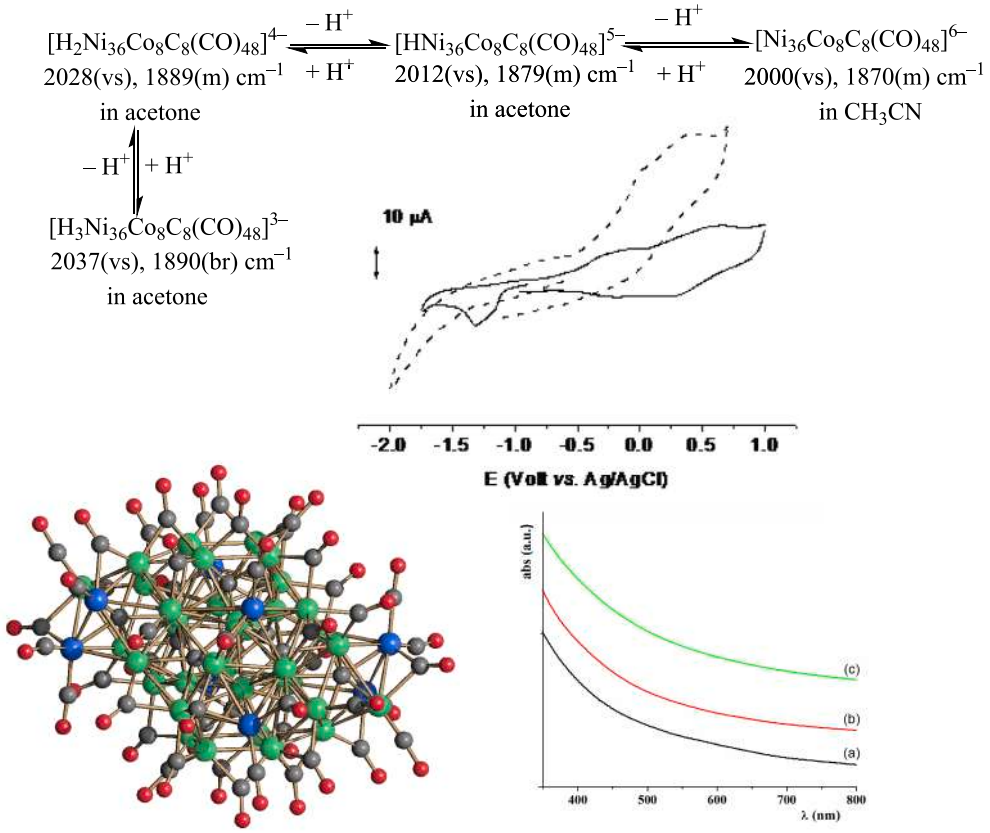

Fig. 27. Protonation/deprotonation reactions and molecular structure of $[H_{6-n}Ni_{36}Co_8C_8(CO)_{48}]^{n-}$ (n = 3–6) (green, Ni; blue, Co; red, O; grey, C). Hydride ligands have not been located by SC-XRD. Cyclic voltammograms recorded at a platinum electrode in CH_3CN solution of $[Ni_{36}Co_8C_8(CO)_{48}]^{6-}$ ($0.8x10^{-3}$ M) (full line) and $[HNi_{36}Co_8C_8(CO)_{48}]^{5-}$ ($1.3x10^{-3}$ M) (dashed line). $[NBu_4][PF_6]$ (0.2 M) supporting electrolyte. Scan rate 0.2 Vs^{-1}. Normalised UV–visible spectra of (a) $[Ni_{36}Co_8C_8(CO)_{48}]^{6-}$ (10^{-5} M in CH_3CN); (b) $[HNi_{36}Co_8C_8(CO)_{48}]^{5-}$ (10^{-5} M in CH_3CN); (c) $[H_2Ni_{36}Co_8C_8(CO)_{48}]^{4-}$ (10^{-5} M in acetone). Adapted from ref. [122] with permission from The Royal Society of Chemistry.

Table 2
Formal redox potentials (V vs. SCE) of some couples of isostructural multivalent hydride and non-hydride MCCs.

	–3/–4	–4/–5	–5/–6	–6/–7	–7/–8	–8/–9	–9/–10
$[HNi_{36}Pt_4(CO)_{45}]^{5-}$		–0.70	–1.08	–1.36	–1.76		
$[Ni_{36}Pt_4(CO)_{45}]^{6-}$			–0.80	–1.15	–1.46	–1.82	
$[HNi_{35}Pt_9(CO)_{48}]^{5-}$	–0.30	–0.73	–1.17	–1.38			
$[Ni_{35}Pt_9(CO)_{48}]^{6-}$		–0.23	–0.63	–1.03	–1.43		
$[HNi_{38}Pt_6(CO)_{48}]^{5-}$	–0.25	–0.62	–0.96	–1.28	–1.62		
$[Ni_{38}Pt_6(CO)_{48}]^{6-}$			–0.62	–0.97	–1.29	–1.54	–1.75
$[HNi_{38}C_6(CO)_{42}]^{5-}$			–0.60	–1.11	–1.42	–1.77	
$[Ni_{38}C_6(CO)_{42}]^{6-}$			–0.49	–0.98	–1.33	–1.73	

hydride MCCs must be sufficiently reactive with the substrate, H^+ or CO_2, in order to generate the desired product. HER selectivity can be ensured just avoiding the presence of CO_2. Conversely, since protons are always present and required in the first chemical reaction, the selectivity for CO_2 reduction depends on the capacity of the hydride MCC intermediate to preferentially transfer the hydride to CO_2 rather than to H^+. Cluster reactivity depends on its charge, size, nature of the interstitial atom, and may be further tuned by replacing some carbonyls with other ligands such as phosphines [30]. For instance, it has been shown that substituted clusters $[Fe_4N(CO)_{11}R]^n$ (R = NO^+, PPh_2-CH_2CH_2-9BBN, $(^{Me}PTA^+)_2$, $(^{Me}PTA^+)_4$, H^+; n = 0, –1, +1, +3; 9BBN = 9-borabicyclo (3.3.1)nonane; $^{Me}PTA^+$ = 1-methyl-1-azonia-3,5-diaza-7-phosphaadamantane) may display anodic shifts of the observed reduction potentials up to 700 mV compared to unsubstituted $[Fe_4N(CO)_{12}]^-$ [171].

The rate of PT is enhanced by many orders of magnitude using larger MCCs, such as $[Co_{13}C_2(CO)_{24}]^{4-}$ (Scheme 9) [163]. This may be attributed to a statistical effect, since it possesses several Co-Co bonds available for protonation. In this sense, it resembles to heterogeneous electrocatalysis, where multiple PT sites are available on the electrode surface. At the same time, the fact that hydrides may easily migrate on the surface of $[Co_{13}C_2(CO)_{24}]^{4-}$ is in keeping with the fluxionality usually observed by ^1H NMR, particularly in larger hydride MCCs. At the same time, this high hydride mobility is reminiscent of the behavior of H-atoms on a metal surface.

Promising applications for reactive capture of CO_2 (RCC) have been recently demonstrated using an integrated system based on $[Fe_4N(CO)_{12}]^-$ as electrocatalyst in a 30:70 solution of monoethanolamine (MEA) and water with added 0.1 M $KHCO_3$ at pH = 7.9 (Scheme 10) [164].

7. Conclusions

Hydride MCCs display a very rich and variegated chemistry. Hydride ligands may be introduced into MCCs as protons (H^+), hydrides (H^-) or

Table 3
Representative examples of catalysis by hydride MCCs.

MCC	Additive, substrate	Reaction	Product (%yield)	Ref
$[HFe_3(CO)_{11}]^-$	CO_2, H_2, alcohol	Formate ester formation	Methyl formate (5.8)	142
$[HFe_3(CO)_{11}]^-$	$(EtO)_2MeSiH$, amides	Dehydration of amides to nitriles	Nitrile products (52–99)	143
$[HFe_3(CO)_{11}]^-$	P_2N_2 ligand, base, ^{i}PrOH, *N*-(diphenylphosphinyl)-imines derivatives	Hydrogenation of imine	Amine products (35–99)	144
$[HRu_3(CO)_{11}]^-$	H_2O, CO	H_2 evolution	H_2 (100)	145
$H_4Os_4(CO)_{12}$	Amine, CO, propylene	WGS	H_2 (270[a])	146
$[HIr_4(CO)_{11}]^-$	Supported on MgO surface	Propane hydrogenolysis	H_2 (not mentioned)	147
$[H_4Ru_4(CO)_{11}(P^b)]$	Tiglic acid	Hydrogenation	2-methyl butyric acid (49–78)	148
$[H_2Ru_3S(CO)_7(PP^c)]$	Tiglic acid	Asymmetric hydrogenation	2-methyl butyric acid (7–100)	149, 150
$[H_4Ru_4(CO)_{11}(PP^c)]$	α,β-unsaturated carboxylic acids	Asymmetric hydrogenation	Chiral saturated carboxylic acids (48–100)	151, 152
$[H_2Ru_3Ir(CO)_{12}]^-$	KO^{t}Bu, ^{i}PrOH, 4-fluoroacetophenone	Transfer hydrogenation	1-(4-fluorophenyl)ethan-1-ol (52–92)	137
$[H_2Ru_3Ir(CO)_{12}]^-$	KO^{t}Bu, ^{i}PrOH, *trans*-cinnamaldehyde	Hydrogenation	Alcohols, aldehyde (20–99)	137
$[HRu_3(CO)_1]^-$	KO^{t}Bu, ^{i}PrOH, 4-fluoroacetophenone	Transfer hydrogenation	1-(4-fluorophenyl)ethan-1-ol (19–82)	137

[a] Activity (moles of H_2 per mole of complex per day). [b] P = chiral binaphthyl-derived mono-phosphiranes. [c] PP = chiral diphosphine of the ferrocene-based Josiphos or Walphos ligand families.

Table 4
Representative examples of catalysis involving H_2 as reagent or product, and using MCCs as catalyst precursors.

MCC	Additive, substrate	Reaction	Product (%yield)	Ref
$Fe_3(CO)_{12}$	Phosphine, ketone substrates	Asymmetric ketone hydrogenation	Alcohol products (66–99)	153, 154
$Ru_3(CO)_{12}$	Amine, CO, H_2O, propylene	Hydroformylation	Aldehydes, alcohol	146
$Ru_3(CO)_{12}$	CO_2, H_2, MeOH	Alkyl formate production	Methyl formate (106*)	155
$Os_3(CO)_{12}$	CO, H_2	CO reduction to methane	Alkane (not mentioned)	156
$Co_3(CO)_9(CPh)$, $Co_4(CO)_{10}(PPh)_2$	CO, H_2, 1-pentene, 2-pentene	Hydroformylation	Aldehydes (99.7–100)	157
$Rh_6(CO)_{16}$	Amine, CO, H_2O, propylene	Hydroformylation	C4 aldehyde (300*) H_2 (1700*)	146
$Ir_4(CO)_{12}$	CO, H_2	CO reduction to methane	Alkane (not mentioned)	156
$Ir_4(CO)_{12}$	Amine, CO, H_2O	Hydroformylation WGS	C4 aldehyde (250*) H_2 (300*)	146
$Ir_6(CO)_{16}$	Zeolite encapsulated	Hydrogenation of CO	Propane (not mentioned)	147
$[Pt_{15}(CO)_{30}]^{2-}$	Amine, CO, H_2O, propylene	Hydroformylation WGS	C4 aldehyde (0.5*) H_2 (700*)	146
$[Pt_{12}(CO)_{24}]^{2-}$	MCM-41 support, methyl pyruvate, acetophenone	Hydrogenation of methyl pyruvate or acetophenone	Not verified (10–40)	158
$[CuRu_6(CO)_{22}]^-$	KO^{t}Bu, ^{i}PrOH, 4-fluoroacetophenone	Transfer hydrogenation	1-(4-fluorophenyl)ethan-1-ol (50–95)	138
$[AgRu_6(CO)_{22}]^-$	KO^{t}Bu, ^{i}PrOH, 4-fluoroacetophenone	Transfer hydrogenation	1-(4-fluorophenyl)ethan-1-ol (71–93)	138
$[AuRu_5(CO)_{19}]^-$	KO^{t}Bu, ^{i}PrOH, 4-fluoroacetophenone	Transfer hydrogenation	1-(4-fluorophenyl)ethan-1-ol (26–77)	138

*Activity (moles of H_2 per mole of complex per day).

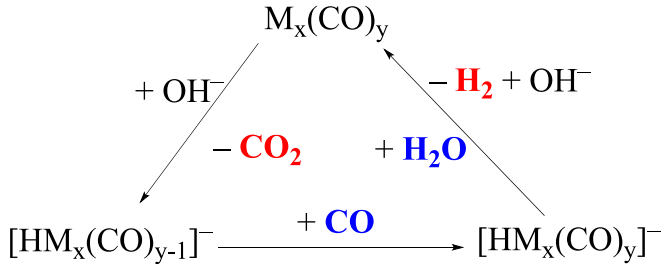

Scheme 5. Mechanism of WGS catalyzed by a MCC.

H-radicals (H·). This reflects the flexibility of hydride MCCs displayed in catalytic and electrocatalytic processes. Nonetheless, often hydrides in MCCs behave as weakly acidic protons and, thus, can be reversibly added/removed by acid/base reactions. In this respect, larger polyhydride MCCs may be viewed as polyprotic acids. The partial positive polarization of hydrogen atoms bonded to MCCs is a consequence of the π-acidity of CO ligands.

Hydride ligands may be found on the surface of the cluster, as well as semi-interstitial or fully interstitial positions. Indeed, H-atoms within structurally characterized hydride MCCs display several different coordination modes, that is, *t*-H, μ-H, μ_3-H (surface of the cluster), μ_4-H (tetrahedral cavity), μ_5-H (square-pyramidal cavity, semi-interstitial), and μ_6-H (octahedral cavity). It must be remarked that location of hydrogens in larger MCCs is not trivial and, thus, it is not possible to rule out the possibility of other coordination modes. Moreover, there is evidence, at least in the case of some lower nuclearity MCCs, of the coordination of H-atoms to the oxygens of CO ligands. Nonetheless, these $[M_n]$–COH species are usually not stable, and rapidly hydrogen migrates to the metal cage. This, somehow, suggests that sometimes protonation of MCCs may initially occur on the CO ligands, followed by rapid migration to the metal cage.

^{1}H NMR studies on lower nuclearity hydride MCCs indicate that hydride ligands are often fluxional, and hydride migration may occur on the surface of the metal cage of the cluster, or through the metal cage itself. These mechanisms have been related to the mobility of H-atoms on a metal surface, and to hydrogen diffusion through a metal, respectively. A further possibility for hydride MCCs is represented by

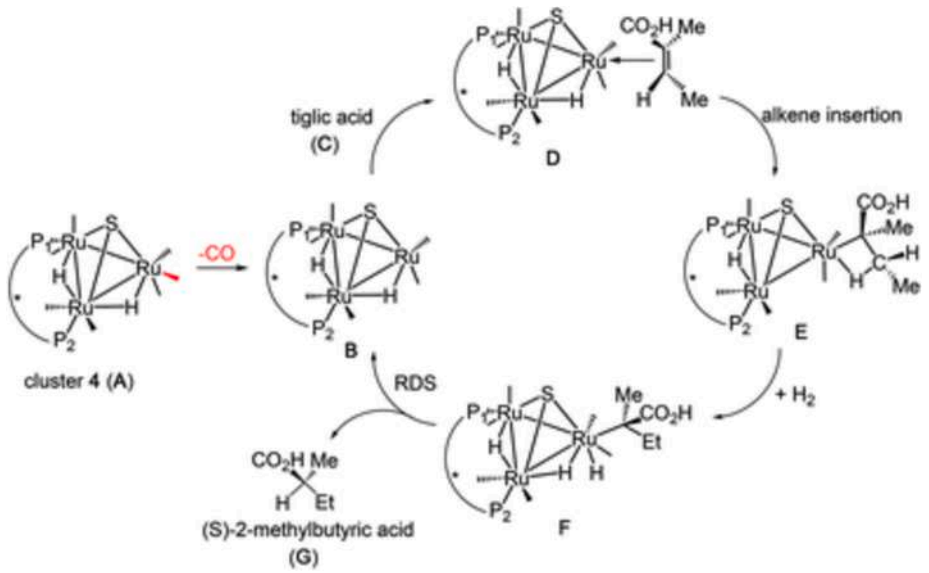

Scheme 6. Computed catalytic hydrogenation cycle of tiglic acid by cluster $[H_2Ru_3S(CO)_7(PP)]$ to give (S)-2-methylbutiryc acid. Reproduced from ref. [148] with permission from The Royal Society of Chemistry.

Table 5
Representative examples of electrocatalysis by MCCs (HER = hydrogen evolution recation; CO_2RR = CO_2 reduction reaction).

MCC	Additive,	Potential (V vs. SCE)	Overpotential (mV)	Reaction	FE* (%)	K_{obs} (s^{-1})	Ref
$[Fe_4N(CO)_{12}]^-$	Benzoic acid	–1.23	280	HER	Quant.	1.0	159, 165
$[Fe_4N(CO)_{12}]^-$	Benzoic acid, CO_2	–1.25	300	CO_2RR	nr	nr	159, 165
$[Fe_4N(CO)_{12}]^-$	MeCN/H_2O (95:5)	–1.25	440	HER	Quant.	nr	165
$[Fe_4N(CO)_{12}]^-$	MeCN/H_2O (95:5), CO_2	–1.2	440	CO_2RR	95	10	165
$[Fe_4N(CO)_{12}]^-$	$KHCO_3/K_2CO_3$ pH 6.5	–1.2	nr	CO_2RR	95	nr	165
$[Fe_4C(CO)_{12}]^{2-}$	Acetate buffer pH 5	–1.25	714	HER	83	368	160, 167
$[Co_{13}C_2(CO)_{24}]^{4-}$	Anilinium tetrafluoroborate	–0.86	760	HER	78	10^8	162, 163
$[HFe_3(CO)_9(\mu_3\text{-pyNH})$	$HBF_4{\cdot}Et_2O$	–1.21	nr	HER	nr	nr	168
$[Fe_3Te_2(CO)_9]$	CF_3COOH	nr	nr	HER	nr	nr	169
$Fe_3MnO(CO)_{12}]^-$	MeCN/H_2O (95:5)	–1.3	540	HER	50	nr	170

*FE = Faradic efficiency. Quant. = quantitative yield, and nr = not reported.

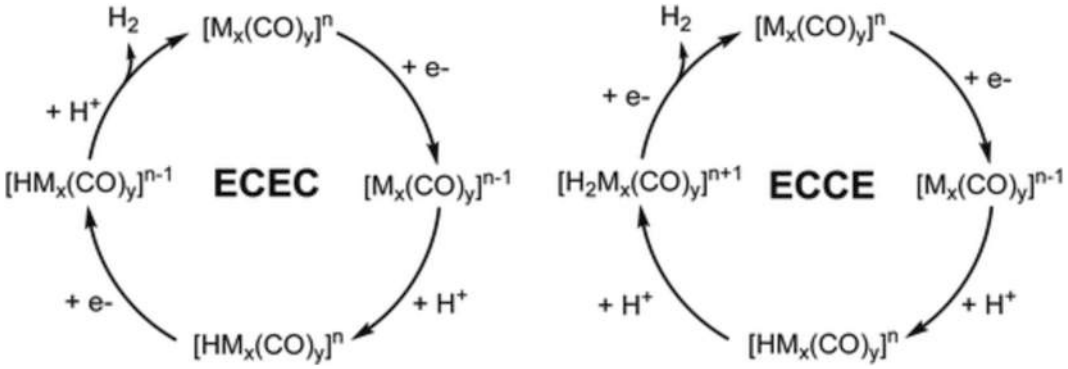

Scheme 7. Examples of electrocatalytic hydrogen-evolution pathway by MCCs. Reproduced from ref. [30] with permission from The Royal Society of Chemistry.

migration involving the metal cage and the O-atoms of the CO ligands. As the nuclearity of the cluster increases, several migration pathways become available to hydride ligands, considerably increasing their mobility. This rapid exchange, together with incipient metallisation of the metal core and onset of paramagnetic properties (on the ground or excited states), might be in part responsible of the problems of detecting hydrides in larger MCCs by ^1H NMR spectroscopy.

The chemistry of larger hydride MCCs is further enriched by the fact that they are often redox active and may display several reversible (or quasi-reversible) redox processes. Therefore, their charges can be variated both by acid-base and redox reactions. Joint chemical, electrochemical and spectroscopic studies are required to unravel these intricate and intriguing systems. As described in Section 5.1, electrochemistry represents also a very useful tool to indirectly prove the hydride nature of larger MCCs. From the other side, acid-base reactions can be used to tune the redox properties of multivalent MCCs.

Finally, hydride MCCs have found several applications in catalysis and, more recently, electrocatalysis [30]. The involvement in catalysis of hydride MCCs can be explained based on their chemical and structural properties reported in this minireview. Regarding electrocatalysis, it has

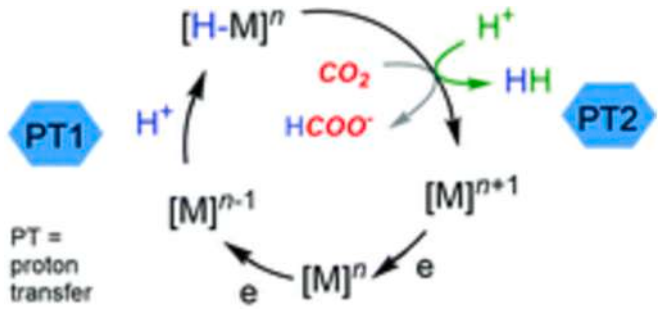

Scheme 8. Schematic showing the two possible reaction pathways for a metal hydride – which can (a) react with protons to form H_2 or (b) react with CO_2 to form formate. Reproduced from ref. [159] with permission from Wiley.

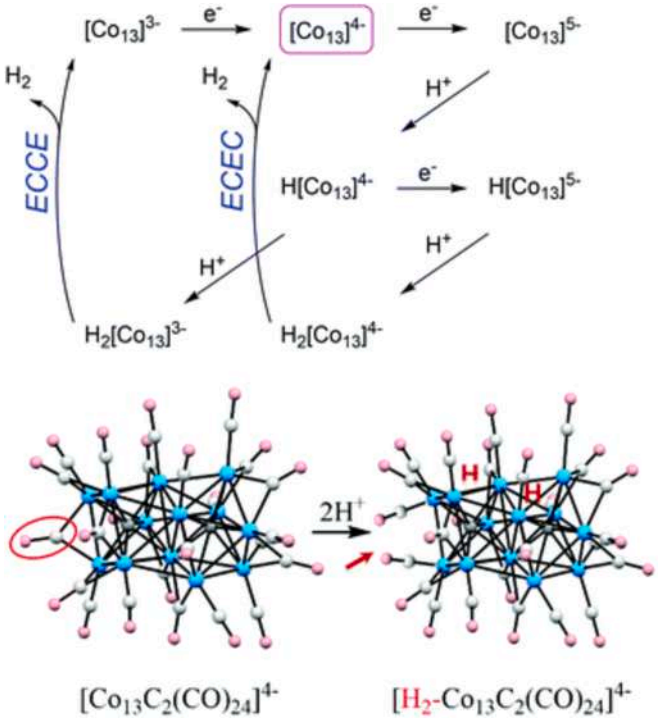

Scheme 9. Top: Proposed mechanism for proton reduction to H_2 in $[Co_{13}C_2(CO)_{24}]^{3-}$; the C and CO ligands are not shown to simplify the mechanistic scheme. Bottom: Protonation of $[Co_{13}C_2(CO)_{24}]^{3-}$ and migration of CO around the cluster core (blue, Co; grey, C; red, O). Reproduced from ref. [159] with permission from Wiley.

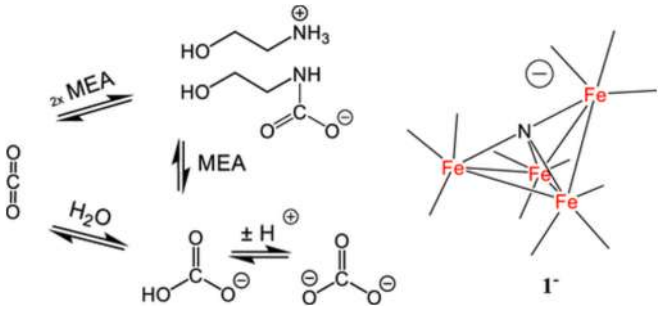

Scheme 10. Representative speciation chemistry for 0.1 M $KHCO_3$ MEA/H_2O (30:70) solutions under 1 arm CO_2 (left), and line drawing of $[Fe_4N(CO)_{12}]^-$ (right). Reproduced with permission from ref. [164] Copyright 2024 American Chemical Society.

been established that formation of hydride MCCs upon electrochemical reduction is crucial in electrocatalytic processes such as hydrogen evolution reaction and CO_2 reduction [159–167,171].

CRediT authorship contribution statement

Cristiana Cesari: Writing – review & editing, Visualization. **Cristina Femoni:** Validation, Writing – review & editing. **Francesca Forti:** Visualization, Validation. **Maria Carmela Iapalucci:** Visualization, Writing – review & editing. **Giorgia Scorzoni:** Visualization, Validation. **Stefano Zacchini:** Conceptualization, Writing – original draft, Writing – review & editing.

Declaration of competing interest

The authors declare that they have no known competing financial interests or personal relationships that could have appeared to influence the work reported in this paper.

Data availability

No data was used for the research described in the article.

Acknowledgements

Financed by the European Union - NextGenerationEU through the Italian Ministry of University and Research under PNRR - Mission 4 Component 1, Investment 4.1 (DM 118/2023) – CUP J33C23002200002. We thank the referees for useful suggestions in revising the manuscript.

References

[1] H. Yu, X. Li, J. Zheng, Beyond hydrogen storage: metal hydrides for catalysis, ACS Catal. 14 (2024) 3139–3157.
[2] J.R. Norton, J. Sowa, Introduction: metal hydrides, Chem. Rev. 116 (2016) 8315–8317.
[3] A. Schneemann, J.L. White, S.Y. Kang, S. Jeong, L.F. Wan, E.S. Cho, T.W. Heo, D. Prendergast, J.J. Urban, B.C. Wood, M.D. Allendorf, V. Stavila, Nanostructured metal hydrides for hydrogen storage, Chem. Rev. 118 (2018) 10775–10839.
[4] G.S. McGrady, G. Guilera, The multifarious world of transition metal hydrides, Chem. Soc. Rev. 32 (2003) 383–392.
[5] J.C. Babón, M.A. Esteruelas, A.M. López, Homogeneous catalysis with polyhydride complexes, Chem. Soc. Rev. 51 (2022) 9717–9758.
[6] S.J. Connelly Robinson, D.M. Heinekey, Hydride & dihydrogen complexes of earth abundant metals: structure, reactivity, and applications to catalysis, Chem. Commun. 53 (2017) 669–676.
[7] A. Albinati, L.M. Venanzi, Transition metal hydrides as ligands, Coord. Chem. Rev. 200–202 (2000) 687–715.
[8] H.D. Kaesz, R.B. Saillant, Hydride complexes of the transition metals, Chem. Rev. 72 (1972) 231–281.
[9] D.R. Aireddy, K. Ding, Heterolytic dissociation of H_2 in heterogeneous catalysis, ACS Catal. 12 (2022) 4707–4723.
[10] C. Copéret, D.P. Estes, K. Larmier, K. Searles, Isolated surface hydrides: formation, structure, and reactivity, Chem. Rev. 116 (2016) 8463–8505.
[11] T.-H. Chiu, J.-H. Liao, R.P. Brocha Silalahi, M.N. Pillay, C.W. Liu, Hydride-doped coinage metal superatoms and their catalytic applications, Nanoscale Horiz. 9 (2024) 675–692.
[12] C. Sun, B.K. Teo, C. Deng, J. Lin, G.-G. Luo, C.-H. Tung, D. Sun, Hydrido-coinage metal clusters: rational design, synthetic protocols and structural characteristics, Coord. Chem. Rev. 427 (2021) 213576.
[13] R.S. Dhayal, W.E. van Zyl, C.W. Liu, Polyhydrido copper clusters: synthetic advances, structural diversity, and nanocluster-to-nanoparticle conversion, Acc. Chem. Res. 49 (2016) 86–95.
[14] W. Hieber, Metal carbonyls, forty years of research, Adv. Organomet. Chem. 8 (1970) 1–28.
[15] P. Braunstein, L.A. Oro, P.R. Raithby (Eds.), Metal Clusters in Chemistry, Wiley-VCH, Weinheim, 1999.
[16] G. Schmid (Ed.), Clusters and Colloids, Wiley-VCH, Weinheim, 1994.
[17] P.J. Dyson, J.S. McIndoe, Transition metal carbonyl cluster chemistry, Gordon and Breach Science Publishers, Amsterdam, 2000.
[18] P. Chini, G. Longoni, S. Martinengo, A. Ceriotti, Relationships between carbonyl hydride clusters and interstitial hydrides, Adv. Chem. 167 (1978) 1–10.
[19] P. Chini, Large metal carbonyl clusters (LMCC), J. Organomet. Chem. 200 (1980) 37–61.

[20] P.R. Raithby, The growth of higher nuclearity carbonyl clusters of ruthenium and osmium, J. Organomet. Chem. 1005 (2024) 122979.
[21] S. Zacchini, Using metal carbonyl clusters to develop a molecular approach towards metal nanoparticles, Eur. J. Inorg. Chem. 4125–4145 (2011).
[22] E.L. Muetterties, T.N. Rhodin, E. Band, C.F. Bruker, W.R. Pretzer, Clusters and Surfaces, Chem. Rev. 79 (1979) 91–137.
[23] R. Bau, M.H. Drabnis, Structures of transition metal hydrides determined by neutron diffraction, Inorg. Chim. Acta 259 (1997) 27–50.
[24] A. Bashall, L.H. Gade, J. Lewis, B.F.G. Johnson, G.J. McIntyre, Direct location of the hydrido ligands in the dianion $[H_4Os_{10}(CO)_{24}]^{2-}$ by a neutron diffraction study of Its $[(Ph_3P)_2N]^+$ salt at 20 K, Angew. Chem. Int. Ed. 30 (1991) 1164–1167.
[25] D.W. Hart, R.G. Teller, C.-Y. Wei, R. Bau, G. Longoni, S. Campanella, P. Chini, T. F. Koetzle, An interstitial hydrogen atom in a hexanuclear metal cluster: X-ray and neutron diffraction analysis of $[(Ph_3P)_2N]^+[HCo_6(CO)_{15}]^-$, J. Am. Chem. Soc. 103 (1981) 1458–1466.
[26] R.W. Broach, L.F. Dahl, G. Longoni, P. Chini, A.J. Schultz, J.M. Williams, Stereochemistry of monohydrido- and dihydrido-dodecanickel carbonyl clusters containing a hexagonal close packed nickel fragment, Adv. Chem. Ser. 167 (1978) 93–110.
[27] P.F. Jackson, B.F.G. Johnson, J. Lewis, P.R. Raithby, M. McPartlin, W.J.H. Nelson, K.D. Rouse, Direct location of the interstitial hydride ligand in $[HRu_6(CO)_{18}]^-$ by both X-ray and neutron analyses of $[Ph_4As][HRu_6(CO)_{18}]$, J. Chem. Soc., Chem. Commun. (1980) 295–297.
[28] R. Bau, M.H. Drabnis, L. Garlaschelli, W.T. Klooster, Z. Xie, T.F. Koetzle, S. Martinengo, Five-coordinate hydrogen: neutron diffraction analysis of the hydrido cluster complex $[H_2Rh_{13}(CO)_{24}]^{3-}$, Science 275 (1997) 1099–1102.
[29] J.M. Bemis, L.F. Dahl, $H_{12}Pd_{28}(PtMe_3)(PtPPh_3)_{12}(CO)_{27}$, a high nuclearity $Pd_{28}Pt_{13}$ cluster containing 12 hydrido atoms: a possible molecular hydrogen-storage model for palladium metal, J. Am. Chem. Soc. 119 (1997) 4545–4546.
[30] C. Cesari, J.-H. Shon, S. Zacchini, L.A. Berben, Metal carbonyl clusters of groups 8–10: synthesis and catalysis, Chem. Soc. Rev. 50 (2021) 9503–9539.
[31] M.D. Vargas, J.N. Nicholls, High-nuclearity carbonyl clusters: their synthesis and reactivity, Adv. Inorg. Chem. Radiochem. 30 (1986) 123–222.
[32] B.F.G. Johnson, J. Lewis, P.R. Raithby, G. Süss, The triruthenium cluster anion $[Ru_3H(CO)_{11}]^-$: preparation, structure and fluxionality, J. Chem. Soc., Dalton Trans (1979) 1356–1361.
[33] J.G. Patrow, Y. Cheng, C.G. Pyles, B. Luo, I.A. Tonks, A.M. Massari, Spectroscopic study of sol-gel entrapped triruthenium dodecacarbonyl catalyst reveals hydride formation, J. Phys. Chem. Chem. Let. 11 (2020) 7394–7399.
[34] C.R. Eady, B.F.G. Johnson, J. Lewis, Synthesis and carbon-13 nuclear magnetic resonance studies of the hexanuclear osmium clusters $[H_2Os_6(CO)_{18}]$, $[Hos_6(CO)_{18}]^-$, and $[Os_6(CO)_{18}]^{2-}$, J. Chem. Soc., Chem. Commun. (1976) 302–303.
[35] L.M. Bavaro, P. Montangero, J.B. Keister, Kinetics and mechanism of oxidative addition and reductive elimination of hydrogen on triruthenium clusters, J. Am. Chem. Soc. 105 (1983) 4977–4981.
[36] L. Garlaschelli, F. Greco, G. Peli, M. Manassero, M. Sansoni, R. Gobetto, L. Salassa, R., Della pergola, synthesis, solid-state structure and multinuclear NMR studies of the new polyhydrido iridium carbonyl cluster $Ir_4H_4(\mu\text{-}H)_4(CO)_4(PPh_3)_4$, Eur. J. Inorg. Chem. (2003) 2108–2112.
[37] S.A.R. Knox, J.W. Koepke, M.A. Andrews, H.D. Kaesz, Synthesis of hydrido- and deuterio-carbonyl cluster complexes of ruthenium, Iron-Ruthenium, and Osmium from Metal Carbonyls and Hydrogen at Atmospheric Pressure 97 (1975) 3942–3947.
[38] R. D. Adams, M. P. Pompeo, W. Wu, Cluster Synthesis. 32. Hydrogen-Rich Metal Cluster Complexes from the Reaction of $Pt_2Os_4(CO)_{18}$ with Hydrogen. Synthesis and Molecular Structures of $PtOs_5(CO)_{16}(\mu\text{-}H)_6$, $Pt_2Os_5(CO)_{17}(\mu\text{-}H)_6$, $PtOs_6(CO)_{18}(\mu\text{-}H)_8$, and $Pt_2Os_7(CO)_{23}(\mu\text{-}H)_8$, Inorg. Chem. 30 (1991) 2425-2432.
[39] C. Allevi, B.T. Heaton, C. Seregni, L. Strona, R.J. Goodfellow, P. Chini, S. Martinengo, Ligand fluxionality in close-packed rhodium carbonyl clusters, J. Chem. Soc., Dalton Trans (1986) 1375–1381.
[40] D. Collini, F. Fabrizi de Biani, D.S. Dolzhnikov, C. Femoni, M.C. Iapalucci, G. Longoni, C. Tiozzo, S. Zacchini, P. Zanello, Synthesis, structure, and spectroscopic characterization of $[H_{8-n}Rh_{22}(CO)_{35}]^{n-}$ (n = 4, 5) and $[H_2Rh_{13}(CO)_{24}\{Cu(MeCN)\}_2]^-$ clusters: assessment of CV and DPV As techniques to circumstantiate the presence of elusive hydride atoms, Inorg. Chem. 50 (2011) 2790–2798.
[41] J.L. Vidal, R.C. Schoening, Rhodium carbonyl cluster chemistry under high pressure of carbon monoxide and hydrogen: VII. Conversion of $[Rh_{15}(CO)_{27}]^{3-}$ into other high nuclearity clusters: new high-yield syntheses for $[Rh_{13}(CO)_{24}H_2]^{3-}$ and $[Rh_{14}(CO)_{26}]^{2-}$, J. Organomet. Chem. 218 (1981) 217–227.
[42] G. Longoni, P. Chini, Synthesis and Chemical Characterization of Platinum Carbonyl Dianions $[Pt_3(CO)_6]_n^{2-}$ (n = ~10, 6, 5, 4, 3, 2, 1). A New Series of Inorganic Oligomers, J. Am. Chem. Soc. 98 (1976) 7225-7231.
[43] B. Berti, C. Femoni, M.C. Iapalucci, S. Ruggieri, S. Zacchini, Functionalization, modification, and transformation of platinum chini clusters, Eur. J. Inorg. Chem. 3285–3296 (2018).
[44] I. Ciabatti, C. Femoni, M.C. Iapalucci, G. Longoni, S. Zacchini, Platinum carbonyl clusters chemistry: four decades of challenging nanoscience, J. Clust. Sci. 25 (2014) 115–146.
[45] C. Cesari, C. Femoni, M.C. Iapalucci, S. Zacchini, Molecular Fe, Co and Ni carbide carbonyl clusters and nanoclusters, Inorg. Chim. Acta 544 (2023) 121235.
[46] R.P. Stewart, U. Anders, W.A.G. Graham, A novel synthesis of $Fe_5C(CO)_{15}$ from the $[Fe_6C(CO)_{16}]^{2-}$ anion, J. Organomet. Chem. 32 (1971) C49–C51.
[47] C. Femoni, M.C. Iapalucci, G. Longoni, S. Zacchini, The chemistry of hydridocarbonylferrates revisited: syntheses and structures of the new $[H_2Fe_4(CO)_{12}]^{2-}$ and $[HFe_5(CO)_{14}]^{3-}$ anions, and the $[Fe(DMF)_4][Fe_4(CO)_{12}(\mu_5\text{-}\eta^2\text{-}CO)(\mu\text{-}H)]_2$ adduct containing an unprecedented isocarbonyl, Dalton Trans. 40 (2011) 8685–8694.
[48] A. Bernardi, C. Femoni, M.C. Iapalucci, G. Longoni, F. Ranuzzi, S. Zacchini, P. Zanello, S. Fedi, Synthesis, molecular structure and properties of the $[H_{6-n}Ni_{30}C_4(CO)_{34}(CdCl)_2]^{n-}$ (n = 3–6) bimetallic carbide carbonyl cluster: a model for the growth of noncompact interstitial metal carbides, Chem. Eur. J. 14 (2008) 1924–1934.
[49] C. Femoni, M.C. Iapalucci, G. Longoni, S. Zacchini, E. Zazzaroni, Synthesis and X-ray structure of the $[\{Fe_3(CO)_9(\mu_3\text{-}O)\}_2H]^{3-}$ trianion: dimerization of a metal carbonyl cluster *via* formation of an exceptionally short hydrogen bond, Dalton Trans. 2644–2651 (2007).
[50] J.-J. Cherng, Y.-C. Tsai, C.-H. Ueng, G.-H. Lee, S.-M. Peng, M. Shieh, New synthesis of $[SFe_3(CO)_9]^{2-}$ and its reactivity toward electrophiles, Organometallics 17 (1998) 255–261.
[51] J.H. Davis, M.A. Beno, J.M. Williams, J. Zimmie, M. Tachikawa, E.L. Muetterties, Structure and chemistry of a metal cluster with a four-coordinate carbide carbon atom, Proc. Natl. Acad. Sci. 78 (1981) 668–671.
[52] H.A. Hodali, D.F. Shriver, C.A. Ammlung, μ-Carbonyl-μ-hydrido-decacarbonyltriferric Acid, $H_2Fe_3(CO)_{11}$, J. Am. Chem. Soc. 199 (1978) 5239–5240.
[53] K.H. Whitmire, D.F. Shriver, $(\mu\text{-}H)Fe_4(CO)_{12}(\eta^2\text{-}COH)$: evidence for a protonated η^2-CO complex as an intermediate in the proton-induced reduction of CO, J. Am. Chem. Soc. 103 (1981) 6754–6755.
[54] J.B. Keister, Rearrangement of O-protonated metal carbonyl clusters. Conversion of $HRu_3(COH)(CO)_{10}$ to $H_2Ru_3(CO)_{11}$, J. Organomet. Chem. 190 (1980) C36–C38.
[55] M.R. Churchill, B.G. DeBoer, Structural studies on polynuclear osmium carbonyl hydrides. 1. crystal structures of the isomorphous species $H_2Os_3(CO)_{11}$ and $Os_3(CO)_{12}$. direct information on the role of an equatorial μ_2-bridging hydride ligand in perturbing the arrangement of carbonyl ligands in a triangular cluster, Inorg. Chem. 16 (1977) 878–884.
[56] H.-N. Adams, G. Facchinetti, J. Strähle, Crystal and molecular structure of $Co_3(CO)_9COH$, a possible intermediate in the reduction of CO by molecular hydrogen, Angew. Chem. Int. Ed. 20 (1981) 125–126.
[57] J.R. Galsworthy, C.E. Housecroft, R.L. Ostrander, A.L. Rheingold, Preparation and characterization of the square-based pyramidal cluster anion $[H_2Ru_5(CO)_{14}(\mu_4\text{-}COH)]$, J. Organomet. Chem. 492 (1995) 211–216.
[58] A. Fumagalli, S. Martinengo, G. Bernasconi, G. Ciani, D.M. Proserpio, A. Sironi, $[Rh_{28}N_4(CO)_{41}H_x]^{4-}$, a massive carbonyl cluster with four interstitial nitrogen atoms, J. Am. Chem. Soc. 119 (1997) 1450–1451.
[59] C. Femoni, M.C. Iapalucci, G. Longoni, S. Zacchini, S. Fedi, F. Fabrizi de Biani, Nickel poly-acetylide carbonyl clusters: structural features, bonding and electrochemical behaviour, Dalton Trans. 41 (2012) 4649–4663.
[60] C. Femoni, M.C. Iapalucci, G. Longoni, S. Zacchini, Polycarbide nickel clusters containing interstitial $Ni(\eta^2\text{-}C_2)_4$ and $Ni_2(\mu\text{-}\eta^2\text{-}C_2)_4$ acetylide moieties: mimicking the supersaturated Ni-C solutions preceding the catalytic growth of CNTs with the structures of $[HNi_{25}(C_2)_4(CO)_{32}]^{3-}$ and $[Ni_{22}(C_2)_4(CO)_{28}Cl]^{3-}$, Chem. Commun. 3157–3159 (2008).
[61] C. Capacci, I. Ciabatti, C. Femoni, M.C. Iapalucci, T. Funaioli, S. Zacchini, V. Zanotti, Molecular nickel phosphide carbonyl nanoclusters: synthesis, structure, and electrochemistry of $[Ni_{11}P(CO)_{18}]^{3-}$ and $[H_{6-n}Ni_{31}P_4(CO)_{39}]^{n-}$ (n = 4 and 5), Inorg. Chem. 57 (2018) 1136–1147.
[62] C. Cesari, I. Ciabatti, C. Femoni, M.C. Iapalucci, S. Zacchini, Capping $[H_{8-n}Ni_{42}C_8(CO)_{44}]^{n-}$ (n = 6, 7, 8) octa-carbide carbonyl nanoclusters with [Ni(CO)] and [CuCl] fragments, J. Clust. Sci. 28 (2017) 1963–1979.
[63] I. Ciabatti, C. Femoni, M.C. Iapalucci, G. Longoni, S. Zacchini, Bimetallic nickel-cobalt hexacarbido carbonyl clusters $[H_{6-n}Ni_{22}Co_6C_6(CO)_{36}]^{n-}$ n = 3–6) possessing polyhydride nature and their base-induced degradation to the monoacetylide [Ni9CoC2(CO)16–x]3– (x = 0, 1), Organometallics 31 (2012) 4593–4600.
[64] D. Collini, F. Fabrizi de Biani, S. Fedi, C. Femoni, F. Kaswalder, M.C. Iapalucci, G. Longoni, C. Tiozzo, S. Zacchini, P. Zanello, Synthesis and electrochemistry of new rh-centered and conjuncto rhodium carbonyl clusters. X-ray structure of $[NEt_4]_3[Rh_{15}(CO)_{27}]$, $[NEt_4]_3[Rh_{15}(CO)_{25}(MeCN)_2]\cdot 2MeCN$, and $[NEt_4]_3[Rh_{75}(CO)_{37}]$, Inorg. Chem. 46 (2007) 7971–7981.
[65] A. Bernardi, C. Femoni, M.C. Iapalucci, G. Longoni, S. Zacchini, S. Fedi, P. Zanello, Synthesis, structures and electrochemistry of new carbonylnickel octacarbide clusters: the distorting action of carbide atoms in the growth of Ni cages and the first example of the inclusion of a carbon atom within a (Distorted) Ni Octahedral Cage, Eur. J. Inorg. Chem. 4831–4842 (2010).
[66] R.D. Adams, B. Captain, J.L. Smith, High-nuclearity iridium carbonyl clusters containing phenylgermyl ligands: synthesis, structures, and reactivity, Inorg. Chem. 44 (2005) 1413–1420.
[67] B.F.G. Johnson, J.G.M. Nairn, D.B. Brown, J. Lewis, M. Gallop, D.G. Parker, The photoisometrisation reactions of the cluster $[Os_3(CO)_9(\mu_3\text{-}\eta^2\text{:}\eta^2\text{-}C_6H_6)]$ and some of its derivatives, Chem. Eur. J. 1 (1995) 211–265.
[68] C. Femoni, M.C. Iapalucci, G. Longoni, S. Zacchini, S. Zarra, New findings in the chemistry of iron carbonyls: the previously unreported $[H_{4-n}Fe_4(CO)_{12}]^{n-}$ (n = 1, 2) series of clusters, which fills the gap with ruthenium and osmium, Inorg. Chem. 48 (2009) 1599–1605.
[69] C. Cesari, M. Bortoluzzi, C. Femoni, M.C. Iapalucci, S. Zacchini, Synthesis, molecular structure and fluxional behavior of the elusive $[HRu_4(CO)_{12}]^{3-}$ carbonyl anion, Dalton Trans. 51 (2022) 2250–2261.

[70] C. Cesari, M. Bortoluzzi, C. Femoni, M.C. Iapalucci, S. Zacchini, One-pot atmospheric pressure synthesis of $[H_3Ru_4(CO)_{12}]^-$, Dalton Trans. 50 (2021) 9610–9622.

[71] R. Ros, A. Tassan, S. Detti, R. Roulet, K. Schenk, Hydrido-derivatives of [Ir4(CO)10(diphosphine)]: X-ray analyses of [Ir4H(CO)9(μ-Ph2PH(CH3)PPh2)]– and [Ir4H(CO)9(μ-Ph2P(CH2)nPPh2)]– (n = 2, 3), Inorg. Chim. Acta 359 (2006) 2417–2423.

[72] M. Bergamo, T. Beringhelli, G. D'Alfonso, L. Garavaglia, P. Mercandelli, M. Moret, A. Sironi, Hydrido-carbonyl rhenium clusters with a square geometry of the metal core. synthesis and X-ray characterization of the novel $[Re_4(\mu\text{-}H)_3(CO)_{16}]^-$ anion, J. Clust. Sci. 12 (2001) 223–242.

[73] M. Bergamo, T. Beringhelli, G. D'Alfonso, P. Mercandelli, M. Moret, A. Sironi, Hydrido-carbonyl chain clusters. synthesis, solid state structure, and solution behavior of the tetranuclear open cluster anions $[Re_4H(\mu\text{-}H)_2(CO)_{17}]^-$ and $[Re_4(\mu\text{-}H)(CO)_{18}]^-$, Organometallics 16 (1997) 4129–4137.

[74] R.D. Adams, Z. Li, J.-C. Lii, W. Wu, C. Synthesis, 40. New high-nuclearity platinum-ruthenium carbonyl cluster complexes. synthesis and structural characterizations of $Ru_8Pt_2(CO)_{23}(\mu_3\text{-}H)_2$, $Ru_7Pt_3(CO)_{22}(\mu_3\text{-}H)_2$, and $Ru_8Pt_2(CO)_{21}(\mu_3\text{-}\eta^2\text{-}CO)_2(dppe)(\mu\text{-}H)_2$ with a new type of triply bridging CO ligand and the new layered cluster complex $Ru_6Pt_3(CO)_{21}(\mu\text{-}CO)(\mu_3\text{-}H)_2$, Organometallics 11 (1992) 4001–4009.

[75] C. Cesari, M. Bortoluzzi, C. Femoni, F. Forti, M.C. Iapalucci, S. Zacchini, Peraurated ruthenium hydride carbonyl clusters: aurophilicity, isolobal analogy, structural isomerism, and fluxionality, Dalton Trans. 53 (2024) 3865–3879.

[76] D. Marabello, F. Bertolotti, G. Gervasio, Hydrogen atoms location in $Os_3(\mu\text{-}H)(CO)_9(\mu_3,\mu^2\text{-}C_2H)$ from accurate X-ray data at 100 K, J. Chem. Crystallogr. 40 (2010) 72–75.

[77] A.G. Orpen, The indirect location of hydride ligands in metal carbonyl clusters, J. Organomet. Chem. 159 (1978) C1–C4.

[78] A.G. Orpen, Indirect location of hydride ligands in metal cluster complexes, J. Chem. Soc., Dalton Trans (1980) 2509–2516.

[79] R.S. Dhayal, J.-H. Liao, S. Kahlal, X. Wang, Y.-C. Liu, M.-H. Chiang, W.E. van Zyl, J.-Y. Saillard, C.W. Liu, $[Cu_{32}(H)_{20}\{S_2P(OiPr)_2\}_{12}]$: the largest number of hydrides recorded in a molecular nanocluster by neutron diffraction, Chem. Eur. J. 21 (2015) 8369–8374.

[80] S.J. La Placa, W.C. Hamilton, J.A. Ibers, A. Davison, Nature of the metal-hydrogen bond in transition metal-hydrogen complexes: neutron and X-ray diffraction studies of β-pentacarbonylmanganese hydride, Inorg. Chem. 8 (1969) 1928–1935.

[81] R.W. Broach, J.M. Williams, Interaction of hydrogen and hydrocarbons with transition metals. neutron diffraction study of Di-μ-hydrido-decacarbonyltriosmium, (μ-H)2Os3(CO)10, containing a four-center, four-electron H2Os2 bond, Inorg. Chem. 18 (1979) 314–319.

[82] A.J. Schultz, J.M. Williams, R.B. Calvert, J.R. Shapley, G.D. Stucky, Interaction of hydrogen and hydrocarbons with transition metals. neutron diffraction study of the crystal and molecular structure of $(\mu\text{-}H)_2Os_3(CO)_{10}(\mu\text{-}CH_2)$, Inorg. Chem. 18 (1979) 319–323.

[83] A.G. Orpen, T.F. Koetzle, Low-temperature X-ray and neutron diffraction studies of tetra-*n*-butylammonium octadecacarbonyl-μ_3-hydrido-*octahedro*-hexaosmium, Acta Cryst. C 43 (1987) 2084–2088.

[84] R. Bau, S.A. Mason, L. Li, W.-T. Wong, Neutron diffraction analysis of $H_2Os_6(CO)_{18}$, J. Am. Chem. Soc. 119 (1997) 11992–11993.

[85] R. Bau, M.Y. Chiang, C.-Y. Wei, L. Garlaschelli, S. Martinengo, T.F. Koetzle, X-ray and neutron diffraction study of $[P(CH_2C_6H_5)(C_6H_5)_3]^+[HIr_4(CO)_{11}]^-$, Inorg. Chem. 23 (1984) 4758–4762.

[86] N. Masciocchi, G. D'Alfonso, W. Kockelmann, W. Schäfer, A. Sironi, Hydrogen atoms location in $[Re_4(\mu_3\text{-}H)_4(CO)_{12}]$ by joint X-ray single-crystal and neutron powder diffraction analysis, Chem. Commun. 1903–1904 (1997).

[87] J. Dong, Z.-H. Gao, Q.-F. Zhang, L.-S. Wang, The synthesis, bonding, and transformation of a ligand-protected gold nanohydride cluster, Angew. Chem. Int. Ed. 60 (2021) 2424–2430.

[88] X. Yuan, C. Sun, X. Li, S. Malola, B.K. Teo, H. Häkkinen, L.-S. Zheng, N. Zheng, Combinatorial identification of hydrides in a ligated ag_{40} nanocluster with noncompact metal core, J. Am. Chem. Soc. 141 (2019) 11905–11911.

[89] R. Della Pergola, L. Garlaschelli, M. Manassero, M. Sansoni, D. Strumolo, Iridium cluster chemistry: the synthesis and the solid state structure of $[HIr_5(CO)_{12}]^{2-}$ and $[HIr_4(CO)_{10}PPh_3]^-$, J. Clust. Sci. 12 (2001) 23–34.

[90] A. Ceriotti, R. Della Pergola, L. Garlaschelli, F. Laschi, M. Manassero, N. Masciocchi, M. Sansoni, P. Zanello, Iron-Iridium Mixed-Metal Carbonyl Clusters. 3. Synthesis, Chemical Characterization, Electrochemical Behavior, and Solid-State Structures of $[NEt_4]_3[FeIr_5(CO)_{15}]$, $[NMe_3(CH_2Ph)]_2[HFeIr_5(CO)_{15}]$, and $[NMe_3(CH_2Ph)]_2[FeIr_5(CO)_{16}]$. Spectroscopic and Chemical Evidence for the Existence of $[HFe_3Ir(CO)_{12}]^{2-}$, $[H_2Fe_3Ir(CO)_{12}]^-$, $[H_2FeIr_5(CO)_{15}]^-$, Inorg. Chem. 30 (1991) 3349-3357.

[91] J.C. Sarker, K.M. Uddin, M.S. Rahman, S. Ghosh, T.A. Siddiquee, D.A. Tocher, M. G. Richmond, G. Hogarth, S.E. Kabir, Bimetallic osmium-tin complexes: Stannylene and hydrostannylene clusters upon addition of Ph3SnH to unsaturated triosmium clusters [(μ-H)2Os3(CO)8(μ-diphosphine)] (diphosphine = dppm, dppf), Inorg. Chim. Acta 409 (2014) 320–329.

[92] S. Deolka, R.R. Fayzullin, E. Khaskin, Bulky PNP ligands blocking metal-ligand cooperation allow for isolation of Ru(0), and lead to catalytically active Ru complexes in acceptorless alcohol dehydrogenation, Chem. Eur. J. 28 (2022) e202103778.

[93] S. Aime, R. Gobetto, E. Valls, Role of Os-H···N-H interactions in directing the stereochemistry of carbonyl cluster hydride derivatives, Organometallics 16 (1997) 5140–5141.

[94] K.E. Inkrott, S.G. Shore, Stepwise deprotonation of $H_4Ru_4(CO)_{12}$: high-yield synthesis and carbon-13 NMR spectra of $H_3Ru_4(CO)_{12}$ and $H_2Ru_4(CO)_{12}^{2-}$, Inorg. Chem. 18 (1979) 2817–2821.

[95] T. Beringhelli, E. Cariati, C. Dragonetti, S. Galli, E. Lucenti, D. Roberto, A. Sironi, R. Ugo, Variable temperature ^{1}H NMR and X-ray diffraction characterisation of $[H_5Os_{10}(CO)_{24}]^-$ obtained in reproducible and high yields by hydrogenation of silica-supported $[Os(CO)_3(OH)_2]_n$, Inorg. Chim. Acta 354 (2003) 79–89.

[96] A. Gourdon, Y. Jeannin, Electrochemistry and X-ray structures of the isoelectronic clusters $[Fe_5C(CO)_{15}]$, $[N(PPh_3)_2][Fe_5N(CO)_{14}]$ and $[NBu_4]_2[Fe_5C(CO)_{14}]$, J. Organomet. Chem. 290 (1985) 199–211.

[97] R. D. Adams, J. E. Babin, J. T. Tanner, Cluster Synthesis. 22. Synthesis and Structural Characterization of $Ru_7(CO)_{19}(\mu\text{-}CNMe_2)(\mu_6\text{-}H)$ Containing an Interstitial Hydride Ligand and $Ru_5(CO)_{12}(PMe_2Ph)_2(\mu_4\text{-}\eta^2\text{-}CNMe_2)(\mu\text{-}H)$ Containing a Quadruply Bridging (Dimethylamino)carbine Ligand, Organometallics 7 (1988) 2027-2033.

[98] B.T. Heaton, L. Strona, S. Martinengo, D. Strumolo, R.J. Goodfellow, I.H. Sadler, Hexanuclear rhodium hydrido-carbonyl clusters, J. Chem. Soc., Dalton Trans (1982) 1499–1502.

[99] M. Bortoluzzi, I. Ciabatti, C. Femoni, M. Hayatifar, M.C. Iapalucci, G. Longoni, S. Zacchini, Hydride migration from a triangular face to a tetrahedral cavity in tetranuclear iron carbonyl clusters upon coordination of $[AuPPh_3]^+$ fragments, Angew. Chem. Int. Ed. 53 (2014) 7233–7237.

[100] M. Manassero, M. Sansoni, G. Longoni, Crystal structure of $[Me_3NCH_2Ph][Fe_4(CO)_{13}H]$. A 'butterfly' metal cluster with an unusually bonded carbonyl group, J. Chem. Soc., Chem. Commun. (1976) 919–920.

[101] J.A. Jensen, D.E. Fjare, W.L. Gladfelter, Crystal and molecular structure of PPN $[HRu_4(CO)_{13}]$, Inorg. Chem. 22 (1983) 1250–1253.

[102] I. Ciabatti, C. Femoni, M. Gaboardi, M.C. Iapalucci, G. Longoni, D. Pontiroli, M. Riccò, S. Zacchini, Structural rearrangements induced by acid-base reactions in metal carbonyl clusters: the case of $[H_{3-n}Co_{15}Pd_9C_3(CO)_{38}]^{n-}$ (n = 0–3), Dalton Trans. 43 (2014) 4388–4399.

[103] B. Berti, I. Ciabatti, C. Femoni, M.C. Iapalucci, S. Zacchini, Cluster core isomerism induced by crystal packing effects in the $[HCo_{15}Pd_9C_3(CO)_{38}]^{2-}$ molecular nanocluster, ACS Omega 3 (2018) 13239–13250.

[104] J.V. Barkley, T. Eguchi, R.A. Harding, B.T. Heaton, G. Longoni, L. Manzi, H. Nakayama, K. Miyagi, A.K. Smith, A. Steiner, Solid state studies (X-ray and ^{1}H-, ^{13}C-NMR) on $(NMe_4)_{4-x}[H_xNi_{12}(CO)_{21}]\cdot S$ (x = 1, S = Me_2CO; x = 2, S = 2THF), J. Organomet. Chem. 573 (1999) 254–260.

[105] C.R. Eady, B.F.G. Johnson, J. Lewis, M.C. Malatesta, P. Machin, M. McPartlin, $[HRu_6(CO)_{18}]^-$: a ruthenium anion having an interstitial H-ligand. X-Ray crystal structures of two modifications, J. Chem. Soc., Chem. Commun. (1976) 945–946.

[106] B.F.G. Johnson, J.S. McIndoe, Spectroscopic and mass spectrometric methods for the characterisation of metal clusters, Coord. Chem. Rev. 200–202 (2000) 901–932.

[107] I. Ciabatti, C. Femoni, M.C. Iapalucci, G. Longoni, S. Zacchini, Tetrahedral $[H_nPt_4(CO)_4(P^{\wedge}P)_2]^{n+}$ (n = 1, 2; P^P = CH_2=C(PPh$_2$)$_2$) cationic mono- and dihydrido carbonyl clusters obtained by protonation of the neutral $Pt_4(CO)_4(P^{\wedge}P)_2$, Organometallics 32 (2013) 5180–5189.

[108] A. Bernardi, C. Femoni, M.C. Iapalucci, G. Longoni, S. Zacchini, The problems of detecting hydrides in metal carbonyl clusters by ^{1}H NMR: the case study of $[H_{4-n}Ni_{22}(C_2)_4(CO)_{28}(CdBr)_2]^{n-}$ (n = 2–4), Dalton Trans. 4245–4251 (2009).

[109] I. Ciabatti, F. Fabrizi de Biani, C. Femoni, M.C. Iapalucci, G. Longoni, S. Zacchini, Metal segregation in bimetallic Co-Pd carbide carbonyl clusters: synthesis, structure, reactivity and electrochemistry of $[H_{6-n}Co_{20}Pd_{16}C_4(CO)_{48}]^{n-}$ (n = 3–6), ChemPlusChem 78 (2013) 1456–1465.

[110] C. Femoni, M.C. Iapalucci, G. Longoni, C. Tiozzo, S. Zacchini, An organometallic approach to gold nanoparticles: synthesis and X-Ray structure of CO-protected $Au_{21}Fe_{10}$, $Au_{22}Fe_{12}$, and $Au_{28}Fe_{14}$, and $Au_{34}Fe_{14}$ clusters, Angew. Chem. Int. Ed. 47 (2008) 6666–6669.

[111] C. Femoni, M.C. Iapalucci, G. Longoni, T. Lovato, S. Stagni, S. Zacchini, Self-assembly of $[Pt_{3n}(CO)_{6n}]^{2-}$ (n = 4–8) carbonyl clusters: from molecules to conducting molecular metal wires, Inorg. Chem. 49 (2010) 5992–6004.

[112] C. Femoni, M.C. Iapalucci, G. Longoni, J. Wolowska, S. Zacchini, P. Zanello, S. Fedi, M. Riccò, D. Pontiroli, M. Mazzani, Magnetic behavior of odd- and even-electron metal carbonyl clusters: the case study of $[Co_8Pt_4C_2(CO)_{24}]^{n-}$ (n = 1, 2) carbide cluster, J. Am. Chem. Soc. 132 (2010) 2919–2927.

[113] C. Cesari, B. Berti, M. Bortoluzzi, C. Femoni, T. Funaioli, F.M. Vivaldi, M. C. Iapalucci, S. Zacchini, From M_6 to M_{12}, M_{19} and M_{38} molecular alloy Pt-Ni carbonyl nanoclusters: selective growth of atomically precise heterometallic nanoclusters, Dalton Trans. 52 (2023) 3623–3642.

[114] C. Cesari, T. Funaioli, B. Berti, C. Femoni, M.C. Iapalucci, F.M. Vivaldi, S. Zacchini, Atomically precise Ni-Pd Alloy carbonyl nanoclusters: synthesis, total structure, electrochemistry, spectroelectrochemistry, and electrochemical impedance spectroscopy, Inorg. Chem. 60 (2021) 16713–16725.

[115] C. Femoni, M.C. Iapalucci, F. Kaswalder, G. Longoni, S. Zacchini, The possible role of metal carbonyl clusters in nanoscience and nanotechnologies, Coord. Chem. Rev. 250 (2006) 1580–1604.

[116] B. Berti, C. Cesari, C. Femoni, T. Funaioli, M.C. Iapalucci, S. Zacchini, Redox active Ni-Pd carbonyl alloy nanoclusters: syntheses, molecular structures and electrochemistry of $[Ni_{22-x}Pd_{20+x}(CO)_{48}]^{6-}$ (x = 0.62), $[Ni_{29-x}Pd_{6+x}(CO)_{42}]^{6-}$ (x = 0.09) and $[Ni_{29+x}Pd_{6-x}(CO)_{42}]^{6-}$ (x = 0.27), Dalton Trans. 49 (2020) 5513–5522.

[117] E. Cattabriga, I. Ciabatti, C. Femoni, T. Funaioli, M.C. Iapalucci, S. Zacchini, Syntheses, structures, and electrochemistry of the defective *ccp* $[Pt_{33}(CO)_{38}]^{2-}$ and the *bcc* $[Pt_{40}(CO)_{40}]^{6-}$ molecular nanoclusters, Inorg. Chem. 55 (2016) 6068–6079.

[118] C. Cesari, B. Berti, T. Funaioli, C. Femoni, M.C. Iapalucci, D. Pontiroli, G. Magnani, M. Riccò, M. Bortoluzzi, F.M. Vivaldi, S. Zacchini, Atomically precise platinum carbonyl nanoclusters: synthesis, total structure, and electrochemical investigation of $[Pt_{27}(CO)_{31}]^{4-}$ displaying a defective structure, Inorg. Chem. 61 (2022) 12534–12544.

[119] G.J. Lewis, J.D. Roth, R.A. Montag, L.K. Safford, X. Gao, S.-C. Chang, L.F. Dahl, M. J. Weaver, Electroactive metal clusters as models of electrode surfaces: vibrational spectroelectrochemistry of seven redox forms of $[Pt_{24}(CO)_{30}]^n$ (n = 0 to –6) and comparison with potential-dependent spectra of CO chemisorbed on platinum, J. Am. Chem. Soc. 112 (1990) 2831–2832.

[120] J.D. Roth, G.J. Lewis, L.K. Safford, X. Jiang, L.F. Dahl, M.J. Weaver, Exploration of ionizable metal cluster-electrode surface analogy: infrared spectroelectrochemistry of $[Pt_{24}(CO)_{30}]^n$, $[Pt_{26}(CO)_{32}]^n$, and $[Pt_{38}(CO)_{44}]^n$ (n = 0 to –10) and comparison with potential-dependent spectra of CO adlayers of platinum surfaces, J. Am. Chem. Soc. 114 (1992) 6159–6169.

[121] A. Bernardi, I. Ciabatti, C. Femoni, M.C. Iapalucci, G. Longoni, S. Zacchini, Ni-Cu tetracarbide carbonyls with vacant Ni(CO) fragments as borderline compounds between molecular and quasi-molecular clusters, Dalton Trans. 42 (2013) 407–421.

[122] I. Ciabatti, F. Fabrizi de Biani, C. Femoni, M.C. Iapalucci, G. Longoni, S. Zacchini, Selective synthesis of the $[Ni_{36}Co_8C_8(CO)_{48}]^{6-}$ octa-carbide carbonyl cluster by thermal decomposition of the $[H_2Ni_{22}Co_6C_6(CO)_{36}]^{4-}$ hexa-carbide, Dalton Trans. 42 (2013) 9662–9670.

[123] C. Cesari, M. Bortoluzzi, T. Funaioli, C. Femoni, M.C. Iapalucci, S. Zacchini, Highly reduced ruthenium carbide carbonyl clusters: synthesis, molecular structure, reactivity, electrochemistry, and computational investigation of $[Ru_6C(CO)_{15}]^{4-}$, Inorg. Chem. 62 (2023) 14590–14603.

[124] F. Calderoni, F. Demartin, F. Fabrizi de Biani, C. Femoni, M.C. Iapalucci, G. Longoni, P. Zanello, Electron-sink behaviour of the carbonylnickel clusters $[Ni_{32}C_6(CO)_{36}]^{6-}$ and $[Ni_{38}C_6(CO)_{42}]^{6-}$: synthesis and characterization of the anions $[Ni_{32}C_6(CO)_{36}]^{n-}$ (n = 5–10) and $[Ni_{38}C_6(CO)_{42}]^{n-}$ (n = 5–9) and crystal structure of $[PPh_3Me]_6[Ni_{32}C_6(CO)_{36}]\cdot 4MeCM$, Eur. J. Inorg. Chem. 663–671 (1999).

[125] S. Fedi, P. Zanello, F. Laschi, A. Ceriotti, S. El Afefey, A joint electrochemical/spectroelectrochemical inspection (and re-inspection) of high-nuclearity platinum carbonyl clusters, J. Solid State Electrochem. 13 (2009) 1497–1504.

[126] C. Femoni, T. Funaioli, M.C. Iapalucci, S. Ruggieri, S. Zacchini, Rh-Sb nanoclusters: synthesis, structure, and electrochemical studies of the atomically precise $[Rh_{20}Sb_3(CO)_{36}]^{3-}$ and $[Rh_{21}Sb_2(CO)_{38}]^{5-}$ carbonyl compounds, Inorg. Chem. 59 (2020) 4300–4310.

[127] C. Cesari, C. Femoni, T. Funaioli, M.C. Iapalucci, I. Rivalta, S. Ruggieri, S. Zacchini, Heterometallic rhodium clusters as electron reservoirs: Chemical, electrochemical, and theoretical studies of the centered-icosahedral $[Rh_{12}E(CO)_{27}]^{n-}$ atomically precise carbonyl compounds, J. Chem. Phys. 155 (2021) 104301.

[128] F. Demartin, F. Fabrizi de Biani, C. Femoni, M.C. Iapalucci, G. Longoni, P. Macchi, P. Zanello, Synthesis, Electrochemistry and Crystal Structure of the $[Ni_{36}Pt_4(CO)_{45}]^{6-}$ and $[Ni_{37}Pt_4(CO)_{46}]^{6-}$ Hexaanions, J. Clust. Sci. 12 (2001) 61–74.

[129] C. Femoni, M.C. Iapalucci, G. Longoni, P.H. Svensson, P. Zanello, F. Fabrizi de Biani, Synthesis, and characterization of ν_3-octahedral $[Ni_{36}Pd_8(CO)_{48}]^{6-}$ and $[Ni_{35}Pt_9(CO)_{48}]^{6-}$ clusters displaying unexpected surface segregation of Pt atoms and molecular and/or crystal substitutional Ni/Pd and Ni/Pt disorder, Chem. Eur. J. 10 (2004) 2318–2326.

[130] F. Fabrizi de Biani, C. Femoni, M.C. Iapalucci, G. Longoni, P. Zanello, A. Ceriotti, Redox behavior of $[H_{6-n}Ni_{38}Pt_6(CO)_{48}]^{n-}$ (n = 4–6) Anions: a series of metal carbonyl clusters displaying electron-sink features, Inorg. Chem. 38 (1999) 3721–3724.

[131] P. Buchwalter, J. Rosé, P. Braunstein, Multimetallic catalysis based on heterometallic complexes and clusters, Chem. Rev. 115 (2015) 28–126.

[132] R.D. Adams, F.A. Cotton (Eds.), Catalysis by Di- and Polynuclear Metal Cluster Complexes, Wiley-VCH, New York, 1998.

[133] R.D. Adams, B. Captain, Bimetallic cluster complexes: synthesis, structures and applications to catalysis, J. Organomet. Chem. 689 (2004) 4521–4529.

[134] J.M. Thomas, B.F.G. Johnson, R. Raja, G. Sankar, P.A. Midgley, High-Performance nanocatalysts for single-step hydrogenations, Acc. Chem. Res. 36 (2003) 20–30.

[135] M.T. Nielsen, R. Padilla, M. Nielsen, Homogeneous catalysis by organometallic polynuclear clusters, J. Clust. Sci. 31 (2020) 11–61.

[136] G. Hogarth, S.E. Kabir, E. Nordlander, Cluster chemistry in the Noughties: new developments and their relationship to nanoparticles, Dalton Trans. 39 (2010) 6153–6174.

[137] F. Forti, C. Cesari, M. Bortoluzzi, C. Femoni, M.C. Iapalucci, S. Zacchini, Heterometallic Ru-Ir carbonyl clusters as catalyst precursors for hydrogenation and hydrogen transfer reactions, New J. Chem. 47 (2023) 19289–19303.

[138] C. Cesari, M. Bortoluzzi, F. Forti, L. Gubbels, C. Femoni, M.C. Iapalucci, S. Zacchini, 2-D Molecular alloy Ru-M (M = Cu, Ag, and Au) carbonyl clusters: synthesis, molecular structure, catalysis, and computational studies, Inorg. Chem. 61 (2022) 14726–14741.

[139] S.A. Kerns, J. Seo, V.M. Lynch, J. Shearer, S.T. Goralski, E.R. Sullivan, M.J. Rose, Scaffold-based [Fe]-hydrogenase model: H_2 activation initiates Fe(0)-hydride extrusion and non-biomimetic hydride transfer, Chem. Sci. 12 (2021) 12838–12846.

[140] G. Hogarth, An unexpected leading role for $[Fe_2(CO)_6(\mu\text{-pdt})]$ in our understanding of [FeFe]-H_2ases and the search for clean hydrogen production, Coord. Chem. Rev. 490 (2023) 215174.

[141] C. Cesari, B. Berti, F. Calcagno, C. Lucarelli, M. Garavelli, R. Mazzoni, I. Rivalta, S. Zacchini, Bimetallic Co-M (M = Cu, Ag, and Au) carbonyl complexes supported by *N*-heterocyclic carbene ligands: synthesis, structures, computational investigation, and catalysis for ammonia borane dehydrogenation, Organometallics 40 (2021) 2724–2735.

[142] G.O. Evans, C.J. Newell, Conversion of CO_2, H_2, and alcohols into formate esters using anionic carbonyl hydrides, Inorg. Chim. Acta 31 (1978) L387–L389.

[143] S. Zhou, D. Addis, S. Das, K. Junge, M. Beller, New catalytic properties of iron complexes: dehydration of amides to nitriles, Chem. Commun. 4883–4885 (2009).

[144] S. Zhou, S. Fleischer, K. Junge, S. Das, D. Addis, M. Beller, Angew. Enantioselective synthesis of amines: general, efficient iron-catalyzed asymmetric transfer hydrogenation of imines, Chem. Int. Ed. 49 (2010) 8121–8125.

[145] J.C. Bricker, C.C. Nagel, A.A. Bhattacharyya, S.G. Shore, Hydride donating properties of $[HRu_3(CO)_{11}]^-$ in the presence of CO; chemistry of ruthenium carbonyl anions relevant to the catalysis of the water gas shift reaction, J. Am. Chem. Soc. 107 (1985) 377–384.

[146] H.C. Kang, C.H. Mauldin, T. Cole, W. Slegeir, K. Cann, R. Pettit, Reductions with carbon monoxide and water in place of hydrogen. 1. hydroformylation reaction and water gas shift reaction, J. Am. Chem. Soc. 99 (1977) 8323–8325.

[147] S. Kawi, J.-R. Chang, B.C. Gates, Cluster catalysis: propane hydrogenolysis catalyzed by MgO-supported tetrairidium, J. Phys. Chem. 98 (1994) 12978–12988.

[148] A.F. Abdel-Magied, M.H. Majeed, M.F. Abelairas-Edesa, A. Ficks, R.M. Ashour, A. Rahaman, W. Clegg, M. Haukka, L.J. Higham, E. Nordlander, Synthesis and characterization of chiral phosphirane derivatives of [(μ-H)4Ru4(CO)12] and their application in the hydrogenation of an α,β-unsaturated carboxylic acid, J. Organomet. Chem. 849–850 (2017) 71–79.

[149] A.F. Abdel-Magied, A.K. Singh, M. Haukka, M.G. Richmond, E. Nordlander, Diastomeric control of enantioselectivity: evidence for metal cluster catalysis, Chem. Commun. 50 (2014) 7705–7708.

[150] A.F. Abdel-Magied, Y. Theibich, A.K. Singh, A. Ragaman, I. Doverbratt, A.K. Raha, M. Haukka, M.G. Richmond, E. Nordlander, Asymmetric hydrogenation of an α-unsaturated carboxylic acid catalyzed by intact chiral transition metal carbonyl clusters – diastereomeric control of enantioselectivity, Dalton. Trans. 49 (2020) 4244–4256.

[151] V. Moberg, R. Duquesne, S. Contaldi, O. Röhrs, J. Nachtigall, L. Damoense, A. T. Hutton, M. Green, M. Monari, D. Santelia, M. Haukka, E. Nordlander, Efficient cluster-based catalysts for asymmetric hydrogenation of α-unsaturated carboxylic acids, Chem. Eur. J. 18 (2012) 12458–12478.

[152] V. Moberg, M. Haukka, I.O. Koshevoy, R. Ortiz, E. Nordlander, Unprecedented enantioselectivity in a cluster-based catalytic system, Organometallics 26 (2007) 4090–4093.

[153] Y.-Y. Li, S.-L. Yu, W.-Y. Shen, J.-X. Gao, Iron-, cobalt-, and nickel-catalyzed asymmetric transfer hydrogenation and asymmetric hydrogenation of ketones, Acc. Chem. Res. 48 (2015) 2587–2598.

[154] Y. Li, S. Yu, X. Wu, J. Xiao, W. Shen, Z. Dong, J. Gao, Iron catalyzed asymmetric hydrogenation of ketones, J. Am. Chem. Soc. 136 (2014) 4031–4039.

[155] D.J. Daresbourg, C. Ovalles, M. Pala, Homogeneous catalysts for carbon dioxide/hydrogen activation. alkyl formate production using anionic ruthenium carbonyl clusters as catalysts, J. Am. Chem. Soc. 105 (1978) 5937–5939.

[156] M.G. Thomas, B.F. Beier, E.L. Muetterties, Metal clusters in catalysis. IV. catalytic hydrogen reduction of carbon monoxide to alkanes, J. Am. Chem. Soc. 98 (1976) 1296–1297.

[157] R. C. Ryan, C. U. Pittman, J. P. O'Connor, Metal Cluster Catalysis. 1. Hydroformylations of 1- and 2-Pentene Catalyzed by Two Cobalt Carbonyl Clusters: $Co_3(CO)_9(\mu_3\text{-}CC_6H_5)$ and $Co_4(CO)_8(\mu_2\text{-}CO)_2(\mu_4\text{-}PC_6H_5)_2$, J. Am. Chem. Soc. 99 (1977) 1986-1988.

[158] S. Basu, H. Paul, C.S. Gopinath, S. Bhaduri, G.K. Lahiri, A MCM-41-supported platinum carbonyl cluster-derived asymmetric hydrogenation catalyst, J. Catal. 229 (2005) 298–302.

[159] N.D. Loewen, T.V. Neelakantan, L.A. Berben, Renewable formate from C-H bond formation with CO_2: using iron carbonyl clusters as electrocatalysts, Acc. Chem. Res. 50 (2017) 2362–2370.

[160] A. Taheri, L.A. Berben, Tailoring electrocatalysts for selective CO_2 or H^+ reduction: iron carbonyl clusters as a case study, Inorg. Chem. 55 (2016) 378–385.

[161] N.D. Loewen, E.J. Thompson, M. Kagan, C.L. Banales, T.W. Myers, J.C. Fettinger, L.A. Berben, A pendant proton shuttle on $[Fe_4N(CO)_{12}]^-$ alters product selectivity in formate *vs.* $_H2$ production the hydride $[H\text{–}F_e4N(CO)_{1}2^]$–, Chem. Sci. 7 (2016) 2728–2735.

[162] C.C. Carr, A. Taheri, L.A. Berben, Fast proton transfer and hydrogen evolution reactivity mediated by $[Co_{13}C_2(CO)_{24}]^{4-}$, J. Am. Chem. Soc. 142 (2020) 12299–12305.

[163] S. Pattanayak, L.A. Berben, Cobalt carbonyl clusters enable independent control of two proton transfer rates in the mechanism for hydrogen evolution, ChemElectroChem 8 (2021) 2488–2494.

[164] R.E. Siegel, M. Aceves, L.A. Berben, Direct electrochemical conversion of CO_2 sorbent solution to formate by a molecular iron catalyst, ACS Energy Lett. 9 (2024) 2896–2901.

[165] M.D. Rail, L.A. Berben, Directing the reactivity of $[HFe_4N(CO)_{12}]^-$ toward H^+ or CO_2 reduction by understanding the electrocatalytic mechanism, J. Am. Chem. Soc. 133 (2011) 18577–18579.

[166] A. Taheri, E.J. Thompson, J.C. Fettinger, L.A. Berben, An Iron electrocatalyst for selective reduction of CO_2 to formate in water: including thermochemical insights, ACS Catal. 5 (2015) 7140–7151.

[167] A.D. Nguyen, M.D. Rail, M. Shanmugam, J.C. Fettinger, L.A. Berben, Electrocatalytic hydrogen evolution form water by a series of iron carbonyl clusters, Inorg. Chem. 52 (2013) 12847–12854.
[168] S. Ghosh, G. Hogarth, Trinuclear clusters containing 2-aminopyridinate/pyrimidinate ligands as electrocatalysts for proton reduction, J. Organomet. Chem. 851 (2017) 57–67.
[169] A. Rahaman, G.C. Lisensky, J. Browder-Long, D.A. Hrovat, M.G. Richmond, E. Nordlander, G. Hogarth, Electrocatalytic proton-reduction behaviour of telluride-capped triiron clusters: tuning of overpotentials and stabilization of redox states relative to lighter chalcogenide analogues, Dalton Trans. 49 (2020) 7133–7143.
[170] M. Tachikawa, J. Stein, E.L. Muetterties, R.G. Teller, M.A. Beno, E. Gebert, J. M. Williams, Metal clusters with exposed and low-coordinate nitride nitrogen atoms, J. Am. Chem. Soc. 102 (1980) 6648–6649.
[171] S. Pattanayak, N.D. Loewen, L.A. Berben, Using substituted $[Fe_4N(CO)_{12}]^-$ as platform to probe the effect of cation and lewis acid location on redox potential, Inorg. Chem. 62 (2023) 1919–1925.